



Analysis of a coastal-trapped wave generated by the 2016 extra-tropical cyclonic system in the Southern Brazilian continental shelf with COAWST modeling system

Luis Felipe Ferreira de Mendonça^{a,1,*}, Antônio Fernando Harter Fetter-Filho^b, Mauro Michelena Andrade^c, Fabricio Sanguinetti Cruz de Oliveira^d, Douglas da Silva Lindemann^e, Rose Ane Pereira de Freitas^e, Rafael Afonso do Nascimento Reis^g, Carlos Alexandre Domingos Lentini^{a,1}, Claudia Klose Parise^f, Daniel Caetano Santos^h

^a Federal University of Bahia – UFBA, Salvador, Brazil

^b Federal University of Santa Catarina - UFSC, Florianópolis, Brazil

^c University of Vale do Itajaí - UNIVALI, Itajaí, Brazil

^d Federal University of Rio Grande - FURG, Rio Grande, Brazil

^e Federal University of Pelotas – UFPEL, Pelotas, Brazil

^f Federal University of Maranhão – UFMA, São Luís, Brazil

^g Federal University of Espírito Santo – UFES, Vitória, Brazil

^h Federal University of Santa Maria – UFSM, Santa Maria, Brazil

ARTICLE INFO

Keywords:

Coupled modeling
Shelf circulation
South Atlantic Ocean
Coastal trapped wave

ABSTRACT

This study used the coupled ocean-atmosphere regional model (COAWST) to evaluate the effect of the trapped wave formed by a frontal system over the Southern Brazilian Continental Shelf (SBCS) during September 2016. The oceanic model was configured for the domain of 20–40°S/40–60°W, with a horizontal resolution of 1/9°, 32 vertical levels, and forced with Global Ocean Sea Physical Analysis and Forecasting Products. The model simulations were compared to remote sensing and tide gauges data, with a correlation higher than 0.78 between the wind and sea level rise data and higher than 0.82 for the wave amplitude and phase. Our results showed the presence of a sea level anomaly propagating northward along the continental shelf at 480 km.day⁻¹, probably associated with the presence of a coastal-trapped wave. The analyzed period consisted of the rapid formation of an extra-tropical cyclone on the model grid, intensifying the south-quadrant winds and the associated Ekman transport. The zonal acceleration and Coriolis terms were strongly associated with the wave crossing, with an amplitude greater than 2.10⁻⁵ m.s⁻². The Coriolis term follows the geostrophic flow induced by the wave crest, with values greater than 4.2 m.s⁻², and a correlation coefficient of 0.82 with the pressure gradient and friction terms. The trapped wave reversed the pressure gradient and the over-shelf flow with a negative geostrophic flow (average westward shelf flow). Our results reinforce the fact that these processes change the physical and chemical seawater properties over the SBCS, changing the mixing layer and fertilizing its shelf waters.

1. Introduction

The Southern Brazilian Continental Shelf (SBCS) is located between the latitudes of 25 °S and 33,74 °S, it is characterized by the frequent crossing, formation, and/or intensification of frontal systems, predominantly from Chile, Argentina, and Uruguay (Gan and Rao, 1991; Hoskins and Hodges, 2005; Reboita et al., 2010; Krüger et al., 2012; Escobar

et al., 2016; Gramscianinov et al., 2019). Several studies have shown that the Southwest Atlantic Ocean has atmospheric and oceanic conditions for cyclogenesis formation. These conditions contribute to an intense exchange of sensible and latent heat between the two systems. These phenomena have been the subject of several studies using observed data, reanalysis, and global and regional models (Bitencourt et al., 2011; Gozzo e Rocha, 2013; Rosa et al., 2013; Gozzo et al., 2014; Rocha et al.,

* Corresponding author.

E-mail address: luis.mendonca@ufba.br (L.F.F. Mendonça).

¹ Tropical Oceanography Group – GOAT.

2018; Reboita et al., 2019; Reboita et al., 2020).

Cyclogenesis are recurring features on the Southwest Atlantic Ocean at mid-latitudes and can be observed throughout the year, being more frequent between May and September (Escobar et al., 2016). The crossing of frontal systems may be accompanied by cyclones and anticyclones, which change the pressure, wind, and other atmospheric variables. Using data from ERA-Interim, Machado et al. (2020) indicated that storms on the southern Brazilian coast are followed by strong winds, causing an intense disturbance on the sea surface. These synoptic systems have highly destructive potential, with winds hitting the coastline, lasting from hours to days. One of the most well-documented phenomena of this kind was the Catarina Cyclone in March 2004. This system generated winds over 150 km.h^{-1} and inflicted considerable damage to the infrastructure of several cities along the southern coast of Brazil. The strong winds associated with these atmospheric systems impacted the sea surface and generated instability in the mixing layer, changing the coastal circulation and transport (Stech and Lorenzetti, 1992; Castro and Lee, 1995; Innocentini and Caetano Neto, 1996; Rocha et al. 2004).

These free surface oscillations are strongly correlated with synoptic and transitional systems, generating variations with periods of days to weeks. The winds on the SBCS are a first-order forcing to the local oceanic circulation, in which the wind stress and Ekman transport are responsible for water dynamics at different time scales (Möller et al., 2008). The local wind accounts for 90 % of sea level changes along the coast. Part of this sea level rise is associated with the meteorological tide (its non-astronomical component), which is defined by the difference between the observed sea level and the predicted astronomical tide (Guimarães et al., 2014). Parise et al. (2009) estimated a maximum meteorological tide of 1.9 m over a beach in southern Brazil during spring. This event presented cyclogenesis in the south of Uruguay, eastward displacement, a pathway between 35°S and 57.5°S , and the formation of a stronger wind fetch, leading to high sea level elevation. In the time scales of this work, the atmosphere can induce sea level variations through two mechanical effects: (i) inverse barometer effect of the atmosphere over the ocean (Wunsch and Stammer, 1997) and (ii) drag (tangential tension) caused by the wind tension on the sea surface (Dean and Dalrymple, 1991).

The circulation over the South Atlantic Ocean is controlled by a high-pressure center associated with the Hadley cell, called the South Atlantic Subtropical High (SASH) (Sun et al., 2017). This system changes seasonally and influences the climate in the southern Brazilian regions, generating connections between SST anomalies and precipitation on the Southwest Atlantic Ocean (SAO) (Diaz et al., 1998). The seasonal winds profile on the SAO is strongly associated with the SASH meridional variation. According to Hoskins and Hodges (2005), the SAO is influenced by extra-tropical cyclones and anticyclones in the South Hemisphere, especially during winter. The Southwest Atlantic Ocean is constantly affected by the cold-air masses and extra-tropical cyclones and the ocean-atmosphere coupling in mid-latitudes, under a strong wind, induces the turbulent mixing and the mass transport of marine currents over the entire SBCS (Camargo et al., 2013).

The SBCS is characterized by a regular morphology that presents a slight slope and establishes a smooth passage to the upper continental slope (Zenbruski et al., 1972). The presence of the Brazil Current characterizes the ocean circulation of the SBCS offshore region, a western boundary current of the subtropical gyre of the South Atlantic Ocean (Matano et al., 2014). The Brazil Current (BC) is formed at approximately 16°S and flows towards south/southwest, along the continental shelf break of South America (Wienders et al., 2000). In the opposite direction to the BC, the Malvinas Current (MC) is a faster current that flows north/northeast parallel to the Argentine shelf break and carries between 40 Sv and 70 Sv (Fetter and Matano, 2008; Matano et al., 2010). The conjunction of these currents occurs at 38°S and the so-called Brazil-Malvinas Confluence (BMC) (Fetter and Matano, 2008; Matano et al., 2010). The shelf circulation consists of a flow of cold waters from the south, transporting the Subantarctic Shelf Water

(SASW) mixed with La Plata River waters, and a warm flow from the north carrying the Subtropical Shelf Water (STSW), that are constantly fed by the BC (Piola et al., 2000; Palma et al., 2008). Subantarctic Shelf Waters have thermohaline characteristics that are different from those transported by the MC and their velocities are substantially smaller (Piola et al., 2010). The local wind regulates the shelf circulation, while the baroclinic transport out of the shelf break is controlled by BC (Palma and Matano, 2009; Matano et al., 2010). During winter, the southerly winds induce mixing of SASW and La Plata River Plume (PRP), forming a strongly seasonal marine current called the Brazilian Coastal Current (BCC) over the north of La Plata River mouth (Souza and Robinson, 2004). This current is forced by the local wind and by the freshwater discharges from the La Plata River (average runoff of $24,000 \text{ m}^3.\text{s}^{-1}$) and the Patos-Mirim Lagoon system (average runoff of $2000 \text{ m}^3.\text{s}^{-1}$), creating a unique thermohaline profile on the Uruguayan continental shelf and the northern SBCS (Matano et al., 2014).

The astronomical tides on the SBCS have mean amplitudes of 0.4 m and 1.2 m for the neap and spring tide periods, respectively. The astronomical tide is mixed with a semi-diurnal predominance that presents height inequalities, and a small tidal amplitude due to its closeness to an amphidromic point (for M2) in the South Atlantic Ocean. In storm surges, we observe the meteorological component raises the sea level 1 m above the predicted astronomical tide (Truccolo et al., 2004). The southern Brazilian is regularly affected by the crossing, formation, and intensification of atmospheric fronts. These transient meteorological systems not only change the temperature, pressure, wind, and wave fields, but they are also responsible for the momentum transfer for the formation of meteorological tides (Wallace and Hobbs, 1977). Meteorological tides are very frequent and have different amplitudes on the southern Brazilian coast (Andrade et al., 2018). Explosive cyclogenesis in the SBCS is the leading cause of storm surges on the coast. These phenomena occur throughout the year and are more frequent in winter. The primary mechanism responsible for the energy transfer from the atmosphere to the ocean is wind stress on the sea surface, which, associated with the Coriolis force, generates the coastal water piling up (Pugh, 1987). Storm surges amplify the erosive processes and flood these coastal regions (Parise et al., 2009).

Significant variations in the coastal sea level are associated with these meteorological events, which induce the generation of coastal-trapped waves (e.g., Kelvin waves) and intensify the coastal currents system. Coastal trapped waves are a class of surface gravity waves that propagate parallel to the shoreline in regions where the bathymetry gradually deepens. These waves arise due to the interaction of incident ocean waves with the complex coastal geometry and associated spatial variations in water depth. Their behavior is predominantly ruled by the Coriolis effect, resulting from the Earth's rotation, the shape of the coastline, and the stratification of water properties. These waves have a characteristic phase velocity, which depends on the depth water column and the frequency of the incident wave and is of great importance in coastal dynamics. Therefore, their understanding is fundamental for coastal engineering and the prediction of sea level responses associated with climate change.

Frandy et al. (1984) analyzed sea level data and found evidence that the observed storm surges were associated with the propagation of coastal-trapped waves. Although their theoretical analysis was for a flat-bottomed ocean, it only allowed the propagation of Kelvin waves. Tang and Grimshaw (1995) analyzed coastal-trapped waves generated by intense atmospheric systems, such as extra-tropical cyclones, and their results show that lower-mode shelf waves dominate these wave fields. They observed that the large-scale response is predominantly due to shelf waves, while Kelvin waves are confined to transient wavefronts. Several studies have, such as Romea and Smith (1983); Pizarro et al. (2001); Camayo and Campos (2006); Echevin et al. (2014); Pietri et al., 2014; Carvajal et al. (2017); Illig et al. (2018); De Freitas et al. (2021), identified low-frequency oscillations associated with coastal trapped waves in South America. Early work by Smith (1978) showed diurnal

level variations propagating harmonically along the Peruvian coast with velocities of 200 km.day^{-1} . De Freitas et al. (2021) investigated the coastal-trapped waves (CTW's) propagation along the Brazilian continental shelf with in-situ data and HYCOM ocean simulation. These authors observed that the energy of CTW's decreases during propagation, due to variations in the width and depth of the continental shelf. Although not many studies investigate the formation of coastal-trapped waves in the SBCS, Saraceno et al. (2005) showed intra-seasonal peaks in the frequencies of SST and chlorophyll, suggesting coastal-trapped waves as a possible mechanism leading to the observed variability. Moreover, Veleda et al. (2012) analyzed data from five moorings in a cross-section at 11°S , which extends up to 100 km into the open ocean. These authors identified equatorward intraseasonal signals propagating at about $285 \pm 63 \text{ km.day}^{-1}$ along the Brazilian shore. They found maximum correlations between the alongshore currents and nearshore meridional wind stress data at the Southeast Brazil Bight between 22°S and 36°S . Furthermore, this region is influenced by synoptic and mesoscale frontal low-pressure systems, which have frequencies of 4 per month, with average speeds of 500 km.day^{-1} (Stech and Lorenzetti, 1992). Meridional winds change from the northeast to the southwest with the passage of a low-pressure system in this region, inducing drastic changes in wind direction and significant disturbances in the ocean, such as mean sea level changes (Campos et al., 1995).

Hoskins and Hodges (2005), when analyzing systems that lasted longer than two days and covered more than 1000 km, concluded that the storm tracks in the Southern Hemisphere (SH) are important for latitudinal transports and the dynamic of the Southern Ocean. This hypothesis was derived from many SH storm track studies that showed the genesis of eastward-moving cyclonic systems at latitudes higher than 25°S . In the years 2008 and 2010, these events caused severe damage to the facilities and operations of the Port of Itajaí and Navegantes due to floods (Casagrande et al., 2017). According to Chelton et al. (2004), the ocean-atmosphere coupling mechanisms are fundamentally different in the small and mesoscale analysis compared to the basin scales processes. Maloney and Chelton (2006) examined climate models to simulate a positive correlation between SST and the magnitude of wind stress at the ocean surface. The lower-resolution global models cannot simulate the exchanges between SST and SSH on the continental shelf (Taguchi et al., 2012). Gronholz et al. (2017) showed that these differences cause notable changes to ecosystem modeling since the coupled ocean-atmosphere model can better determine coastal circulation. In addition, the atmospheric circulation components simulate local circulation patterns and exchange processes much more effectively (Cocke and Larow, 2000). In addition, works such as Bender et al. (1993), Woollings et al. (2012), Zambon et al. (2014), Meza-Padilla et al. (2015), and Castro and Lee (1995) showed the importance of model coupling for analyzing energy exchanges in studies of storm tracks.

Based on this, we use a coupled ocean-atmosphere model to simulate a strong extra-tropical cyclone formed over the Southwest Atlantic Ocean, near the La Plata River, from September 12 to 15, 2016. This cyclone induced a high-water elevation on the coast, initially in the La Plata River mouth, next to the Uruguayan coast, transferring its energy across the SBCS like a coastal-trapped wave. In this event, southern Brazilian cities, like Florianópolis and Itajaí, had several flooding areas. Although 2015; 2016 showed a strong positive correlation to the El Niño-South Oscillation (ENSO) phase, there is no evidence of a cyclogenesis increase associated with this phenomenon (Ambrizzi et al., 2004). The simulation results were used to investigate the impacts of energy transfer from the atmosphere to the SBCS waters, and the sea level variability produced along the coastal region during the crossing of the frontal system.

1.1. Study case

The analysis of atmospheric conditions was done using synoptic charts from the Center for Weather Forecast and Climate Studies

(CPTEC-INPE) from September 10 to 18, 2016 (available at <http://tempo.cptec.inpe.br/cartas.php?tipo=Superficie>). Fig. 1 describe the synoptic system track from the extra-tropical cyclone's birth to its offshore displacement on 09/15/2016. A low-pressure center was observed on 09/12/2016 when this system moved zonally (close to 32°S) from Argentina towards Brazil. Afterward, the low-pressure center moved southeastwards (00 h on 9/13/2016), at this point as an extra-tropical cyclone on the east coast of Argentina, as indicated by the letter "a". On 09/13/2016, the cyclone intensified to the east of the Argentinean city of Mar del Plata. Sea level pressure ranged from 996 hPa at 00 h to 975 hPa at 00 h on 9/14/2016, with a pressure drop of 21 hPa in 24 h, which was classified as a kind of explosive cyclogenesis (Dal Piva et al., 2011; Reale et al., 2019; Schosler et al., 2020).

The strong southwest winds arrived on Argentina and Uruguay coast on 09/13/2016 (Fig. 1 orange triangles "a" to "d"), reaching up to 24 m.s^{-1} at 18 h. The intense southwest winds on 9/13/2016 piled the waters up at the mouth of the La Plata River against the Uruguayan coast. The southern coast of Rio Grande do Sul State (Brazil) felt an extra-tropical cyclone with winds from the west quadrant and $10\text{--}12 \text{ m.s}^{-1}$. According to the National Institute of Meteorology (INMET), 30–40 mm of accumulated rainfall was registered due to the cold front passage associated with this extra-tropical cyclone. On 09/14/2016, the extra-tropical cyclone moved offshore, and the winds on the Rio Grande do Sul coast began to intensify, reaching 14 m.s^{-1} at 12 h, when the cyclone was at the "f" position (Fig. 1A). At 18 h on 9/14/2016, when the extra-tropical cyclone was at the "g" position, the southern coast of Santa Catarina was hit by winds influenced by the low-pressure system, with speeds close to 10 m.s^{-1} . More intense winds were observed on the southern part of Santa Catarina coast at 06 h on 09/15/2016, while the cyclone was moving offshore (letter "j"), with an average wind speed between 10 and 14 m.s^{-1} (Fig. 1B), the system lost strength during the day, reaching 10 m.s^{-1} at 18 h on 9/15/2016. At this point, the cyclone was out of the study region. On the 09/15/2016 afternoon, the INMET meteorological station, located in Florianópolis (A806), Santa Catarina State (28.60°S - 48.81°W), recorded winds with speeds between 10 and 11 m.s^{-1} . The correlation coefficients of surface wind speed and sea level pressure data measured by the WRF and weather station during the passage of the extra-tropical cyclone (12–September 15, 2016) were 0.57 and 0.97, respectively.

The wind direction and intensity for the studied period, comparing the data obtained through the outputs atmospheric model and the INMET automatic meteorological station of Florianópolis (Fig. 2). The significant wind direction variation of the meteorological station required filtering the high-frequency data (Fig. 2a – black arrow). Through these data we observe the local weather pattern during the extra-tropical cyclone crossing. The Brazilian southern, without the influence of synoptic frontal or cyclogenesis events, is characterized by north/northeast winds associated with SASH. We can observe a balance of intensities between the zonal and meridional components (Fig. 2 b/c). The coupled atmospheric model output shows a similar dynamic observed by the Florianópolis meteorological station. Including the frontal segment, marked on 13/09, which represented the turbulence of the atmospheric baroclinic gradient satisfactorily. The results show that the near-surface flow and turbulence parameters spatially represented the horizontal processes. According to Gibbs et al. (2011), the WRF model predictions generally overestimated the contribution to turbulence generation by mechanical over-buoyancy forcing and parameterization schemes need to represent observational data. Filtering the u and v components of the model shows that the energy distribution is equivalent, even though the resulting wind flow is predominantly meridional (see Fig. 3).

It allows a better understanding of the impact of the Ekman transport and the meteorological tidal's contribution. The largest variations in sea level and wind intensity were analyzed on a synoptic time and spatial scale for the study region. The west cyclone's border remained active on the Santa Catarina coast until 09/16/2016, with intensifying winds from

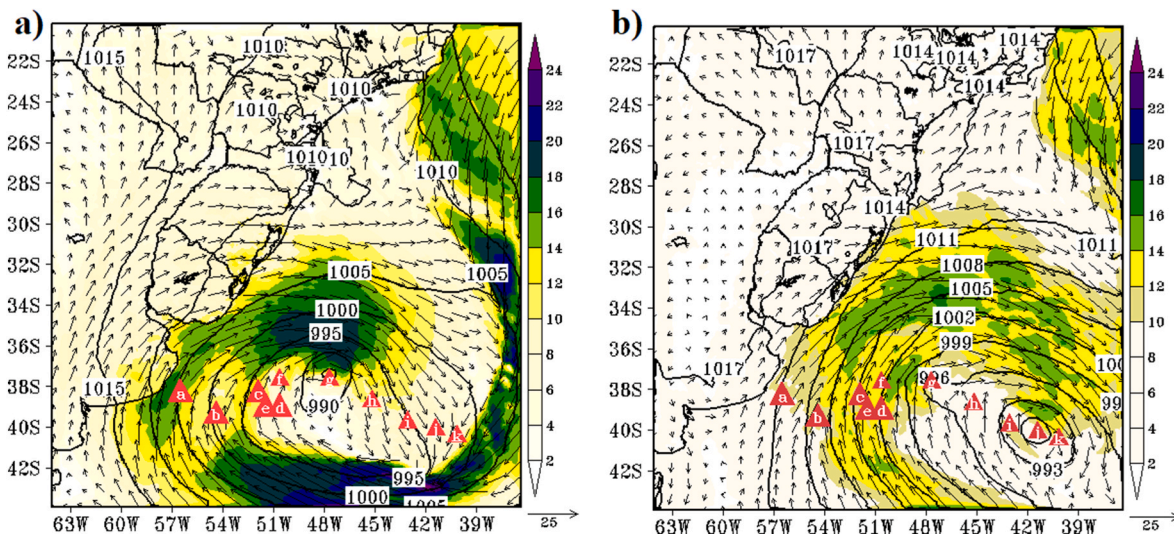


Fig. 1. Extra-tropical cyclone near the southern Brazil, Uruguay, and Argentina coasts during September 12–15, 2016: a) 12 h on 9/14/2016; b) 06 h on 9/15/2016. Red triangles are the cyclone core every 6 h, “a” represents 00 h on 09/13/2016, and “k” represents 12 h on 09/15/2016. Vectors show the wind speed and direction (m s^{-1}), areas filled with magnitude, and black lines indicate the pressure at sea level (hPa).

the south-southwest (S-SW) quadrant. After 09/16/2016, the extra-tropical cyclone lost strength and moved southeastward of the study area, maintaining its high pressure until 09/18/2016. The low-frequency sea level component has an hourly relationship with southern coastal winds and rising sea level. As expected, there is a ~ 6 h delay between the start of the wind action and the change in sea level.

2. Materials and methods

2.1. Numerical simulation

Despite the acceptable performance of some global models to simulate the local conditions, the oceanic signatures of SBCS require a regional model. It represents the exchange processes between the ocean and the atmosphere (Perlin et al., 2011). Gronholz et al. (2017) showed that the interactions in the mixing layer, during and after the crossing of a synoptic system, in an uncoupled simulation, with lower spatial resolution do not satisfactorily represent the shelf environments. In turn, a coupled simulation can settle the trade processes with a higher data resolution. Therefore, this study uses a coupled ocean-atmosphere model system to better represent the complex shelf dynamics during the 2016 frontal systems crossing. The model’s setup and the validation methodology were based on Mendonça et al. (2017) and Do Vale Silva et al. (2018). The understanding of coastal processes is largely based on numerical models, which mathematically reproduce the dynamic conditions of a region of interest.

This study uses the coupled ocean-atmosphere modules from the *Coupled Ocean Atmosphere Wave Sediment Transport* (COAWST) model system (Warner et al., 2008). The ocean module is composed of the *Regional Ocean Modeling System* (ROMS) (Haidvogel et al., 2000; Shchepetkin and McWilliams, 2005, 2009), and the atmospheric module is the *Weather Research and Forecast* (WRF Model Version 4.0.3). The WRF is a non-hydrostatic, fully compressible atmospheric model, with a range of parameterizations of terrain-following mass-based, hybrid sigma-pressure vertical coordinate based on dry hydrostatic pressure, with vertical grid stretching permitted (Powers et al., 2017). The WRF was set up with the same ocean grid area, with 12 km horizontal resolution and 38 isobaric vertical levels. We use the Micro Physics Option in *WRF Single-moment 3-class and 5-class Schemes* (Hong et al., 2004). The Planetary Boundary Layer Scheme is Yonsei University Scheme (YSU) (Hong et al., 2006), with the Kain–Fritsch Scheme (2004) cumulus parameterization. Shortwave and longwave parameterization are the

Dudhia (1989) and RRTM (Mlawer, et al., 1997), respectively, whereas the Land Surface option is NOAH (Niu et al., 2011). According to Kleczek et al. (2014), the adequate time for a spin-up is estimated based on the initialization conditions, and the official WRF website recommends a 12 h turnaround time as the initial state. In this study, the model spin-up lasted 24 h and two days before the occurrence of the extra-tropical cyclone object of this study. The model was integrated for 198 h with a time step of 72s an output interval of 3 h, according to the empirical calculation described by Skamarock et al. (2008).

ROMS is a three-dimensional regional ocean model with a free surface that uses the finite-difference method, solving the Reynolds-Medium and Navier-Stokes equations with the Boussinesq and the hydrostatic approximations. The model uses an Arakawa-C grid with a mask for coast delimitation and sigma vertical coordinates (Shchepetkin and McWilliams, 2005). The oceanic model was configured to a grid with $1/9^\circ$ horizontal resolution and 32 vertical levels. The grid was intended to solve the mesoscale shelf circulation and the set-up/set-down mechanisms associated with the winds on the SBCS. The south open boundary grid includes the La Plata River circulation, while the north open boundary was set to avoid edge instabilities. The initial conditions are from Copernicus - GLOBAL Ocean Sea Physical Analysis and Forecasting Products (GLOBAL_ANALYSIS_FORECAST_PHYS_001_024 - Global Ocean $1/4^\circ$ Physics Analysis and Forecast Updated Daily), available at <https://resources.marine.copernicus.eu>. At the three open boundaries (N–S–E, Fig. 2), the solution was nudged to data from the same Copernicus Product, imposed every hour at a horizontal resolution of $1/4^\circ$. The bathymetry used was from the ETOPO1 - Global Relief Model (Amante and Eakins, 2009) provided by the National Centers for Environmental Information (NCEI). The tidal harmonic components (M2, S2, N2, K2, Q1, O1, P1, K1, M4, MS4, and MN4) from the tidal model OSU TOPEX/Poseidon Global Inverse Solution (TPXO) (Egbert and Erofeeva, 2010), version 7.2, were applied at the open boundaries. A 5-year spin-up was run from October 09, 2011 to October 09, 2016, with initial and boundary conditions from Mercator Global Analysis Forecast and forced by CFSv2 This process continued until the solution reached a quasi-equilibrium state, as Kantha and Clayson (2000) suggested. The final spin-up conditions were used as the initial condition in the oceanic model of COAWST to run the simulations from 2016 September 10 to 18, with hourly outputs subsequently validated according to the following methodology. To perform the coupled simulation, we adjust the model’s frequency information exchange via Bulk-type parameterizations every 300s.

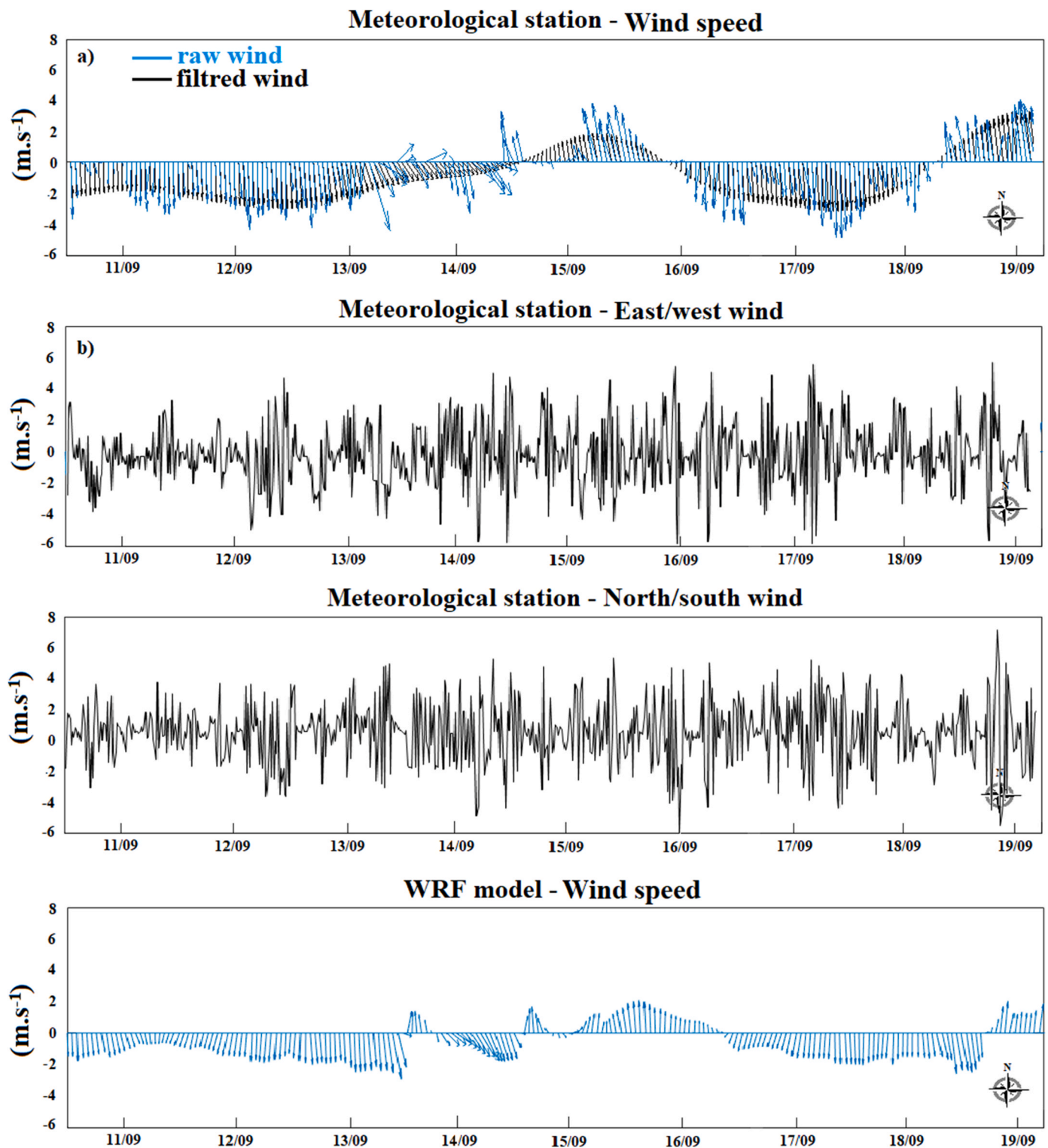


Fig. 2. a) INMET meteorological station in the Florianópolis city (A806) - the blue arrows indicate raw data wind speed ($m.s^{-1}$), and the black arrows are the low frequency filtered wind data b) East/West meteorological station data c) North/South meteorological station data d) wind intensity and direction from the WRF output model at the same position of the INMET meteorological station.

2.2. Heat balance

To analyze the impact of frontal systems on the SBCS region, it is necessary to know the circulation mechanisms compatible with heat flow and mass conservation in the ocean. In order to verify the heat transport within the study grid, the volume transport ($1 Sv = 10^6 m^3.s^{-1}$)

and heat (Terawatt = $10^{12} W$) were calculated along the Rio Grande do Sul and Santa Catarina continental shelves. The oceanic heat transport was computed based on Bryan (1962):

$$\text{Heat transport} \approx \int_0^L \int_{-H}^0 C_p T \rho v dz dx$$

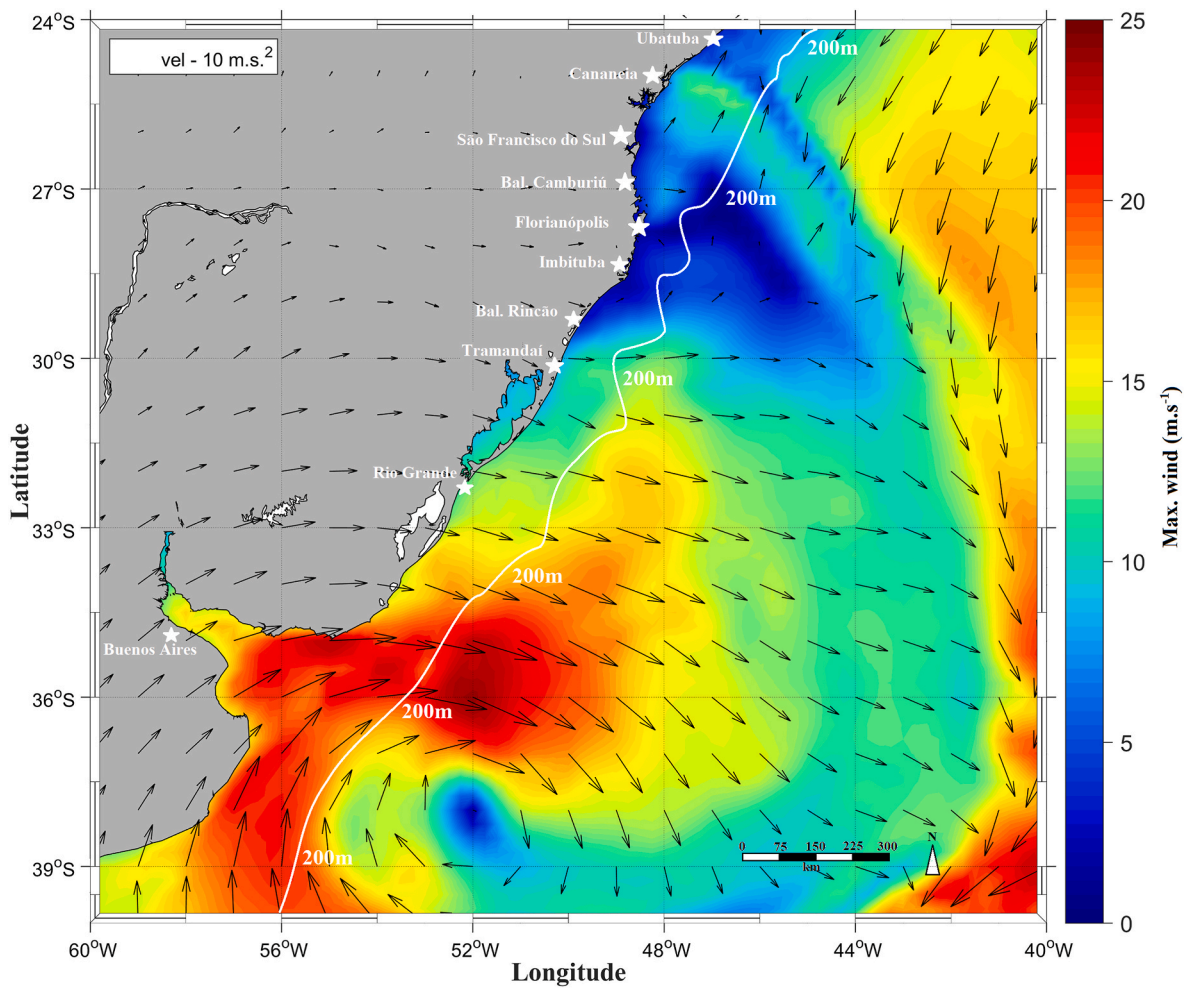


Fig. 3. Modeled study area. The cyclone wind velocity (intensity in colors) and its direction for September 13, 2016. The white line indicates the 200 m shelf break isobath.

where the integral (dx) is taken through the section (from 0 to L), (dz) constitutes the depth integral from the ocean bottom to the surface (from 0 to $-H$), (C_p) is the seawater specific heat, (ρ) is the density, (T) is the potential temperature, and (u, v) are the velocity components normal to the section. The energy transport was calculated for the north, south, and east (200 m shelf break) walls encompassing the Rio Grande do Sul and Santa Catarina coasts. Variations in the heat transport through the boundaries change the total heat content within the grid, indicating the frontal system's impact on the SBCS thermal structure. The total heat content was obtained by calculating the heat integral within the grid volume as follows:

$$\text{Ocean heat content} \approx \int_0^x \int_0^y \int_{-H}^0 C_p T \rho dV$$

where (C_p) is the seawater specific heat, (ρ) is the density, and (T) is the estimated potential temperature within the individual volume (V) of each grid cell. The oceanic heat content was integrated over the entire oceanic volume of the grid during the period under study.

2.3. Validation model

Two data validations were performed to assess the model's hindcast accuracy. The first compares the model's sea surface temperature (SST) and sea surface height (SSH) with remote sensing data. The SST data used are from the *Optimum Interpolation Sea Surface Temperature* (OISST), version 2 (Reynolds et al., 2007), which is a global daily

product from the *National Oceanic and Atmospheric Administration* (NOAA). The Optimum Interpolation (OI) by the *Advanced Very High-Resolution Radiometer* (AVHRR) sensor (Pathfinder versions 5.0 and 5.1) combining observations from satellites, ships, and buoys on a regular global grid with a horizontal resolution of $1/4^\circ$ (Casey et al. 2010). The SSH data were from the *Near-Real Time and Delayed Time* products, from AVISO, at $1/4^\circ$ resolution, available at <https://www.aviso.altimetry.fr>. These data are a global daily product from the *Center National d'Études Spatiales* (CNES) and are estimated by computing time window centered at six weeks, before and after the acquisition date. The data acquisition was performed through a sequence of ten daily images that corresponded to the period from September 10 to 20, 2016. The data were stored without pre-processing and resized to the same grid points from the ocean model to perform a pixel-by-pixel comparative analysis. Validating the model's SST outputs with OISST data showed an average bias of 0.21°C and a standard deviation of 1.3. The high RMSE near the BMC demonstrates the model's lack of skill in reproducing the mesoscale variability of the BMC, as described by Souza and Robinson (2004). The comparison between satellite SSH and modeled free surface ranged between -0.2 and 0.2 m on the SBCS and offshore, close to those found by Hermes and Reason (2005). The typical high-frequency periodicity in tidal data may combine with the lower sampling frequency of the altimeter and cause distortions or associated errors, which can lead to low-frequency artificial signals in the sampled time series (Strub et al., 2015). This concern with tidal errors is more significant when tidal amplitudes are large (Palma et al., 2004, 2008), although errors can occur in conditions like the study area.

The second validation step was comparing the model's free surface height with the tide gauges elevation from the University of Hawaii Sea Level Center (UHSLC, 2022) and the Agricultural Research and Rural Extension of Santa Catarina (EPAGRI) tide gauges at the ten locations described below, during the cyclone formation and crossing. The hourly sea level data were measured at ten tide gauges from Mar del Plata (Argentina) to Ubatuba (Brazil): (1) Mar del Plata (34.66 °S - 58.5 °W); (2) Cananéia (25.01 °S 47.92 °W) and (3) Ubatuba (23.5 °S - 45.11 °W); (4) the Rio Grande data (32.13 °S 52.10 °W) are provided by the Rio Grande Pilotage Port; Tramandaí Pilotage provides (5) the Tramandaí data (29.98 °S 50.13 °W); tide gauges of (6) Balneário Rincão (28.83°S – 49.23 °W), (7) Imbituba (28.13 °S - 48.40 °W), (8) Florianópolis (27.59°S – 48.54°W), (9) Balneário Camboriú (27.00 °S – 48.63 °W), and (10) São Francisco do Sul (26.20 °S – 48.50 °W). We use the model output grid position, nearest the tide gauges position, to analyze the astronomical tide and subtidal components from September 10 to 18, 2016. The raw data were processed using a Lanczos-Cosseno low-pass filter (Thompson, 1983), to remove 95% of oscillations lower than 40 h⁻¹. This process is responsible for isolating the high-frequency (tidal) from low-frequency (subtidal) components associated with an active meteorological system. Based on the distinction between tidal and subtidal data, the comparison, and the statistical analysis of Bias and RMSE were performed during the period of interest.

Fig. 4 shows the low-frequency components (i.e., subtidal, continuous line) of all datasets obtained using a low-pass Lanczos filter at 39 h, which corresponds to the local inertial period. Supratidal oscillations (Fig. 4, dashed line) were obtained by subtracting the subtidal frequencies from the raw series. There is a correlation between coastal winds and sea level, with significant coherence between all frequencies. The most considerable differences appeared at high frequencies; however, the model could simulate with reasonable efficiency the mean subtidal oscillations (Pearson correlation = 0,78), which are mainly forced by the alongshore wind. These oscillations induce a cross-shelf barotropic gradient geostrophically balanced by the alongshore currents (Thompson, 1981; Stech and Lorenzetti, 1992). The modeled free surface values for the Ubatuba and Cananéia sites showed a low sea level rise, without characterizing the trapped wave in the low-frequency component. We observed that the coastline position north of São Francisco do Sul, combined with a broad continental shelf, dissipated the modeled wave energy. Furthermore, in Ubatuba and Cananéia, the M2 tide component is dominant, and its frequency overcomes the modeled free surface. According to Gill (1982), the response of ocean waters to the generating tide force is equal to the solution of long-wave equations forced on the spherical surface, in rotation, with complex bottom and borders. In simple terms, the amplitude of astronomical tide at a coast point depends on the astronomical tide waves amplitude at the edge of the continental shelf, which depends on the distance to the amphidromic points and shelf characteristics.

Despite the high-frequency storm surge daily oscillations, the meteorological tide component significantly impacted sea level rise in this region. Truccolo et al. (2004) show that low-frequency sea level oscillations play an important role along the SBCS because of its microtidal astronomical components. It is even possible to observe the augmentation of the neap tide during the period when the N-NE winds are prevailing in the region. The low-frequency coastal wave is shown in Fig. 4, with tide gauge and model outputs following the extra-tropical cyclone wind fields (S-SW). This process seems responsible for the formation and/or intensification of these waves on SBCS. We can observe similar periods for maximum amplitudes in the comparative analysis between the tidal data and the numerical model. However, in Balneário Rincão and Balneário Camboriú, the model overestimates the observed sea level up to 0.1 m. We believe these differences may be associated with the coastline position where the samples were taken (more external areas). Based on the velocity signal along the coast, there are similarities in the energy distribution between stations through a coherence and phase relationship along the SBCS. Fig. 4 shows a qualitative agreement

between the tide gauge and output model data. However, some significant differences exist in SSH signal propagation towards the north. The model shows a fast wave propagation speed than the *in-situ* observation. The tide gauge data also shows an amplitude reduction in Ubatuba, due to the shelf width reduction shelf above 24 °S as described by De Freitas et al. (2021), after crossing Florianópolis and Balneário Camboriú (less than 100 km to the north). We observed a 12 h anticipation of the wave's appearance at the Cananéia and Ubatuba stations. As the sources differ from EPAGRI data, we believe it could be a data recording error since the wave should appear after the southern stations.

3. Results and discussion

The analysis of the model's free surface verification outputs (Fig. 5) shows us that at 00 h, on 09/14/2016, the displacement of a sea surface elevation anomaly that originated at the Uruguayan coast spreads northward. The surface elevation anomalies analysis, with grid rotation, shows that the extra-tropical cyclone winds intensified the coastal-trapped wave, which continued to propagate towards the Santa Catarina state even after the winds ceased (09/15/2016 -18 h). Melo et al. (2008) showed that extra-tropical cyclones formed near the Brazilian coast could reach it and induce significant sea-level changes. Recently, De Freitas et al. (2021) investigated the trapped coastal waves along the Brazilian continental shelf, between 34 and 11°S, using *in-situ* data combined with the results of a HYCOM high-resolution ocean simulation. According to these authors, the synoptic atmospheric systems are the main mechanisms responsible for triggering these coastally trapped waves along the continental shelf of southeastern Brazil, indicating high energy and coherent periods between 3.5 and 28 days (Filippo, et al., 2012; Dottori and Castro, 2018; De Freitas et al., 2021).

The SSH anomalies associated with the storm surge without the influence of the astronomical tide are shown in Fig. 5. It is possible to estimate the average wave speed through the signal time displacement and covered distance. We use the distance along the sites and consider that the peak of maximum correlation indicates the wave time lag. The La Plata River is the born place as the region where the winds originated or intensified the amplitude of the analyzed trapped wave. The numerical model generated a coefficient of determination in the range of 78%, slope of the regression line close to the ideal value (1.00) with a standard deviation of less than 0.10 m. According to Brink (1991), models tend to underestimate by 10–50% the amplitude of observed fluctuations in the alongshore currents and sea levels. Wave propagation velocity analyses showed higher velocity values (~10–6 m.s⁻¹) over the Uruguayan and Rio Grande do Sul (BR) continental shelves. From Imbituba until Paranaguá, the speed decreased to ~6 m.s⁻¹ due, we believe, to changes in coastline direction, slope reduction, and the widening of the continental shelf. The phase speed decreases over time with the slow winds from the extra-tropical cyclone.

In our study, the physical mechanism that explains the coastal shelf waves' force over topography is straightforward: the dynamic atmospheric pressure response and wind stress along the coast result in Ekman layer transport. Then mass conservation generates a compensating offshore flow in the lower layer. As this flow crosses the isobaths, it changes the local relative vorticity and the alongshore variability. As a result, it generates wave propagation (Brink, 1991). In the southern hemisphere, topographic Rossby waves propagate with the coast at its left, thus progressing to the north along the western continental margin of South America. Gill and Clarke (1974), Schumann (1983), and Battisti and Hickey (1984) were the first works to argue that the alongshore wind stress component is the creator and enhancer of such trapped waves. Consequently, those waves share the same periods with the meteorological systems that caused them. The winds generated by the cyclones' low-pressure gradient centers are the main modulating mechanisms of favorable sea-level variations (Calliari et al., 1988).

The formation process of trapped waves generated at low frequency by atmospheric systems is induced by Proudman resonance (Proudman,

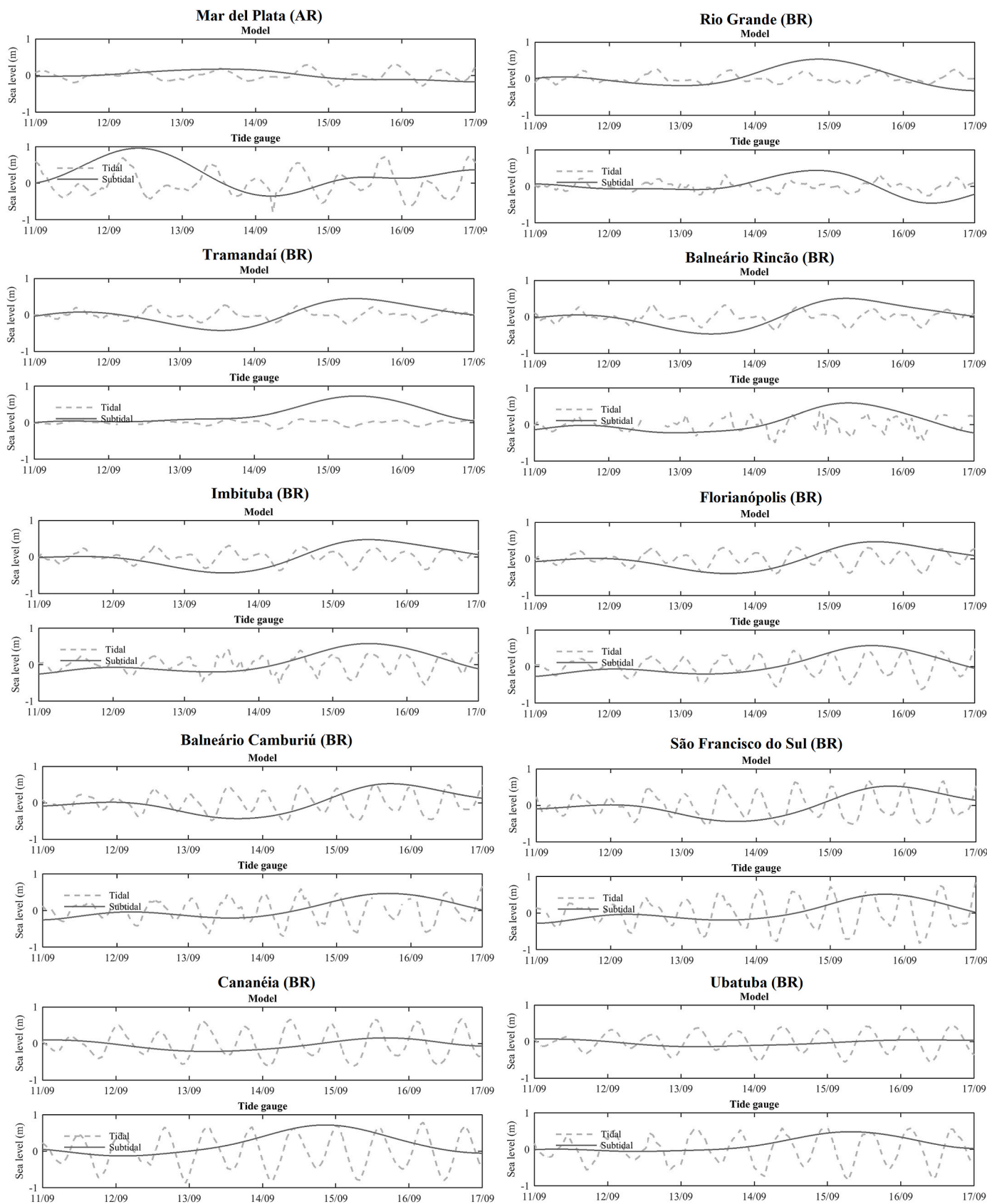


Fig. 4. Tidal and subtidal components from the numerical model and the ten tide gauges along the shore's locations during the trapped wave crossing analyzed period.

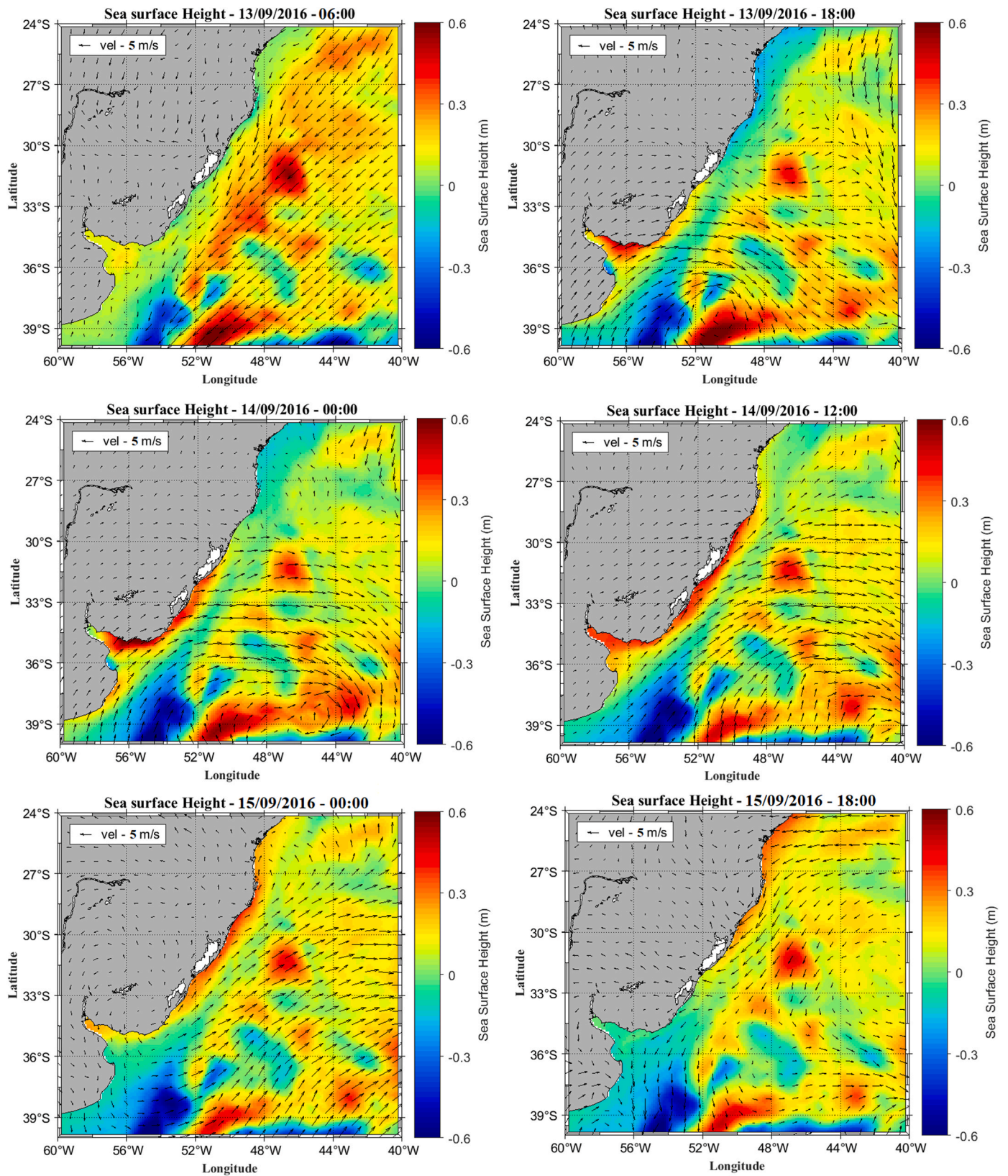


Fig. 5. Maps of the subtidal components of sea surface height and wind fields generated by the ocean model, at specific dates, during the crossing of the frontal system.

1929). This amplification mechanism, also observed in meteorological tsunamis, occurs when the atmospheric component velocity is equal to the shallow water wave velocity (\sqrt{gH}) (Williams et al., 2021). Consequently, the linear increase in the height of a shelf wave with distance is often inferred by Proudman resonance. The effect of tides, sloping bathymetry, velocity, amplitude, and the relationship of atmospheric forcing to the amplitude of the resonant Proudman wave is investigated using analytical approximations and numerical models (Vilibić, 2008). Works such as Bubalo et al. (2018) and Doms et al. (2021) show the potential of using numerical ocean models to map convective systems capable of generating shelf waves via the Proudman resonance. In our study case of mobile pressure fields, the resonance occurs when the displacement speed of atmospheric pressure coincides with the speed propagation of an ocean-free wave (Proudman, 1929; Vennell, 2010). The question is addressed by Pugh (1987), on page 196, for a constant depth, neglecting the rotation and stratification, non-linear effects, and the friction of the water with the bottom. The result of this analysis is the equation (dynamic response = static response/($1-C_a^2/gD$)), in which C_a is the propagation speed of an atmospheric pressure disturbance, and gD is its counterpart for an ocean-free wave. Thus, as the pressure field increases, the sea level response grows to the limit allowed by friction. This resonance mechanism by moving atmospheric pressure pulses has been used to explain the existence of shelf waves with longer periods.

Tang and Grimshaw (1995) showed that transient atmospheric systems could induce coastal water accumulations formed through the geostrophic flow generated by coast-trapped waves. The analysis of the extra-tropical cyclone indicates that the atmospheric system generated a sea level variation by two mechanical effects: (i) atmospheric pressure on the ocean (normal tension) and (ii) drag caused by the wind tension on the sea surface (tangential stress). Works such as Tilburg and Garvine (2004); Parise et al. (2009); Hoeke et al. (2013); Lionello et al. (2019); Lee et al. (2021); Rabinovich et al. (2022) show that in intense atmospheric conditions, the effect of the inverted barometer can raise sea level tens of centimeters. The sea level rise started in the La Plata estuary after the fast development of the extra-tropical cyclone low-pressure core offshore, as shown in Fig. 6a. The atmospheric pressure drops quickly, from 1008 hPa (09/12/2016–12 h) to 990 hPa 24 h later. The sea level response to surface atmospheric pressure follows the inverse barometer effect (Pontes and Gaspar, 1999) with maximum values in the cyclone's core (Fig. 6b) and ~ 0.2 m near Mar del Plata (AR). Fig. 6c shows that at 18 h, on 09/13/2016, in the La Plata River mouth, the SSH was approximately 0.5 m. Therefore, which leads us to believe that southerly winds made the water rise through momentum transfer, not the inverse barometer effect.

Fig. 7 shows the Hovmöller diagrams with the temperature (vertically integrated above 200 m) and free sea surface (no tides) from September 11 to 19, 2016. This figure was generated through an alongshore transect from Florianopolis city (0 m–48,4 °W) until the 200

m isobath (-47.4 °W) to evaluate the water column temperature changes during the crossing of a trapped wave over the continental shelf. Cases 1, 2, and 3 show a sea level variation that occurred with a 12 h delay and vertical temperature inversions, associated with barotropic gradients. Case 2 shows the wind change direction from north-northeast (N-NE) to south-southwest (S-SW) after 12 h on 09/13. It leads to an increase in sea surface elevation at 00 h on 09/14, with a consequent reverse on the thermal structure of the shelf water after 00 h on 09/15 in Florianopolis. The same pattern is observed at the beginning of 09/19 (Case 3), with the winds shifting to the south quadrant, not studied in this manuscript. We believe that the vertical temperature change (Case 1), during 11–12/09, may have been caused by the downwelling in sea surface height by the trench that preceded the crest of the trapped wave studied. The coherent pattern of the subtidal component of the free surface, generates a geostrophic flow described by Houghton and Beer (1976), Brink (1991), Battisti and Hickey (1984), Yao et al. (1984), Kitade and Matsuyama (2000) and Junker et al. (2019).

In order to analyze the thermohaline structure changes during the trapped wave crossing and in which the exchanges between the shelf and offshore area occur, we show the T/S scatter diagram. In spring, the South Antarctic Shelf Water (SASW) over 35 °S indicates a slow retraction of the Brazilian Coastal Current (BCC). The T/S diagram data points corresponding to the SASW and STSW were concentrated at the edges of the characterization boxes, showing that the mixing occurs gradually over the continental shelf, as demonstrated by Möller et al. (2008) and Mendonça et al. (2017). Fig. 8 shows the T/S scatter modeled data for the Rio Grande do Sul continental shelf, before and during the extra-tropical cyclone. The observed density changes in PPW and STSW waters indicate that coastal trapped waves can be responsible for vertical exchanges in the shelf. Pingree and Mardell (1981) show that wind-induced upwelling increases phytoplankton growth. It can occur under improved light conditions, where nutrients and phytoplankton are released into surface waters along the shelf break region. The grid points statistical analysis showed an increase of 8% in the total volume of STSW on the continental shelf. This process shows that an increase in turbulence in the shelf waters can be a crucial mechanism for adding nutrients to the water column, directly impacting primary productivity, as described by Alcaraz et al. (2002) and Saldanha-Corrêa and Gianesella (2004).

The vertical density over the continental shelf (50 nautical miles offshore), from -37.5 °S (Argentina) to -25.5 °S (Brazil) is shown in Fig. 9. We present the 6-hourly vertical thermohaline structure from 06 h (Local Time) on 09/13/2016. A well-defined pycnocline between 20 m and 40 m depth generates a barotropic gradient over the SBCS before the passage of the synoptic system (Fig. 9a). After 6 a.m., on the 14th, the coastal wave propagation reached the southern Brazilian cities of Chuí and Rio Grande, inducing vertical mixing. This process breaks the pycnocline and generates a turbulent layer over the local shelf. According to

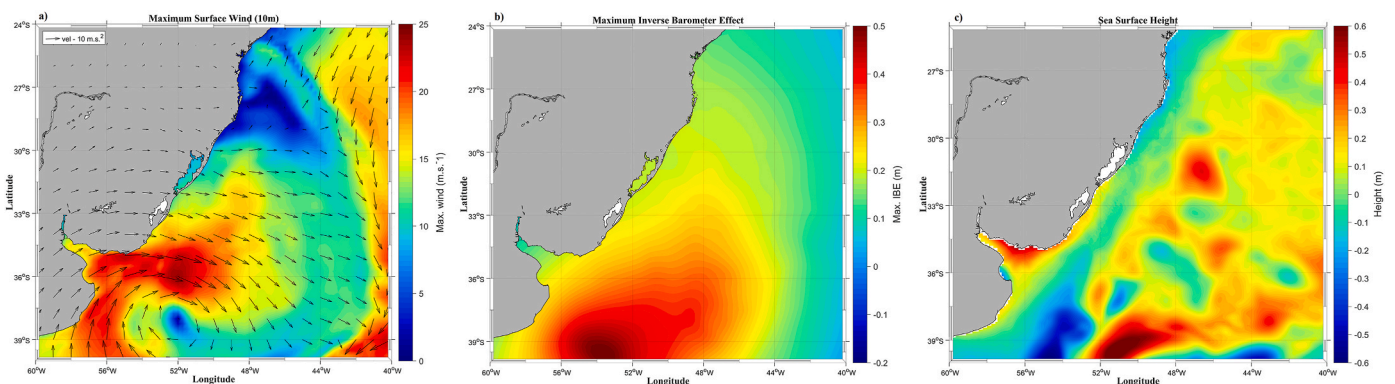


Fig. 6. Non-tidal sea level local driver. (a) Maximum surface wind speed ($\text{m}\cdot\text{s}^{-1}$); (b) Maximum inverse barometer effect (meters); and (c) Maximum modeled sea surface height (meters).

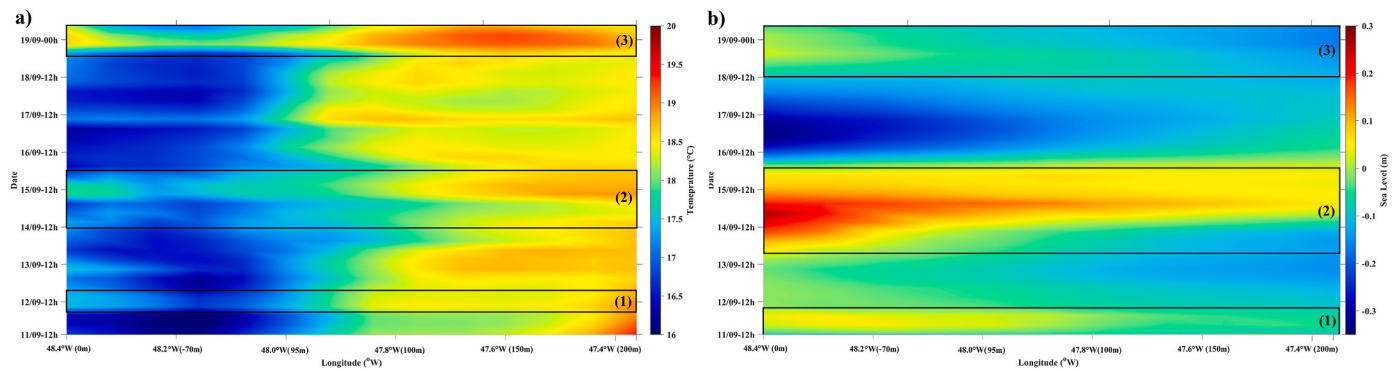


Fig. 7. Hovmöller diagrams with (a) vertically integrated temperature ($^{\circ}\text{C}$) above 200 m and (b) free sea surface height with no tides, in meters, from September 11 to 19, 2016. These diagrams were generated through an alongshore transect from Florianópolis city ($0\text{ m}-48.4^{\circ}\text{W}$) to the 200 m isobath (-47.4°W). Cases 1, 2, and 3 are situations where temperature changes due the sea level variations have been vertically integrated.

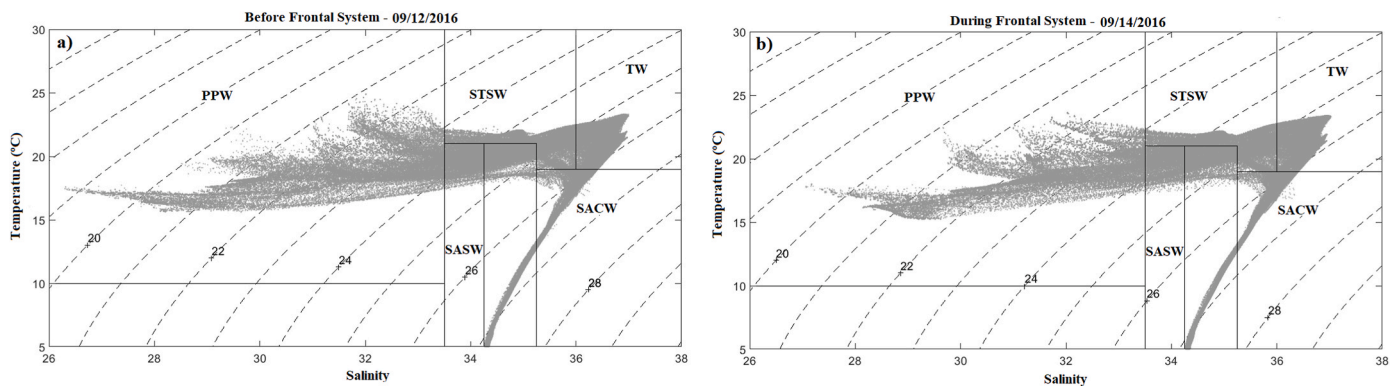


Fig. 8. T/S scatter diagrams with model output data (gray dots) over the SBCS. Shaded lines represent sigma-T values (density). The names of the water masses and thermohaline limits were described by Möller et al. (2008).

Babanin (2006), vertical mixing can be induced by a non-breaking wave, enhancing the mixing layer in the upper ocean. Therefore, further investigation of wave-current and wave-turbulence interactions is paramount to improving our understanding of shelf and cross-shelf vertical mixing processes. However, this is beyond the scope of this study. Indeed, the modeled vertical stratification indicates that the SBCS has a barotropic response to wind-generated disturbances, according to De Freitas et al. (2021). The vertical water column areas north of Florianópolis remained stratified, even after the passage of the trapped waves. We believe that the change in the coastline orientation and rapid depth increase induces potential vorticities, and the exchanges become zonal (east-to-west). According to Palma et al. (2004), there are significant differences in the vertical structures on the shelf north of Florianópolis. In this region, the vertical structure is almost uniform, forced by the wind along the coast, which creates a pressure gradient and an associated geostrophic flow. Before and after the wave passing, disturbances are concentrated on the ocean surface and above the thermocline (upper 40 m).

The vertical momentum component (w) during the trapped wave crossing on the Southwest Atlantic Continental shelf is shown in Fig. 10, under northeast wind conditions, the SBCS is fed by the STSW, due to lateral inputs of the BC tropical water over the shelf, at lower latitudes (Mendonça et al., 2017). At 6 h on 09/13, the continental shelf is stratified with settling velocities near $0.6 \cdot 10^{-4} \text{ m.s}^{-1}$. On 09/14 the overwash, caused by the coastal trapped wave, had the highest amplitudes over the Chui, Rio Grande, Mostardas, and Tramandai (Brazil). The barotropic gradient of this wave changes the vertical mixing, and positive vertical velocity values are observed. According to Musgrave (2019), even a Kelvin wave does not have its purely barotropic flow over the coastal bathymetry and stratified waters, as it includes small

baroclinic components on the bottom and over the shelf break. Green and Coco (2014) analyzed the wave-induced resuspension and sediment transport, including the bottom stresses. During 09/15 (06 h Local time), we observed that the wave trough induces negative velocities to $2.10^{-4} \text{ m.s}^{-1}$, with vertical transport towards the bottom. Fig. 10E shows that after the downward turbulent flow of the mixing layer (wave trough), the turbulence associated with the bottom shear generates resuspension of bottom material. These processes increase continental shelf fertilization and sediment resuspension since the mixing over the shelf can generate turbulence induced by instability in the flow (Rippeth et al., 2005). These vertical mixing processes in coastal waters reveal a dynamic continental shelf, since the passage of frontal systems capable of generating these waves is recurrent, especially in winter.

The zonal transport shows the exchanges between the continental shelf and offshore. Previous studies (Lima and Castello, 1995; Resgalla et al., 2001; Rintoul and England, 2002, Soares et al., 2011) consider Ekman transport associated with the seasonal wind and the baroclinic residuals created by freshwater discharge currents as the primary cross-shelf exchange mechanisms. Fig. 11 shows the zonal transport over the shelf break from the La Plata River (Argentina) up to the north of São Francisco do Sul (Brazil). Fig. 11a shows that the La Plata River and Patos Lagoon discharges dominate the thermohaline and zonal shelf transport, with speeds of up to 0.4 m.s^{-1} in an easterly direction, as described by Piola et al. (2008). In the upwelled waters over the Uruguayan coast (Fig. 11B), the potential energy increase accelerates the geostrophic flow with velocities higher than 0.6 m.s^{-1} . We observe that the trapped wave generates cross-shelf water exchanges towards offshore (crest) and towards onshore (trough), predominantly above 20 m. It is due to the lower salinity surface viscosity of the La Plata River and Patos Lagoon plumes.

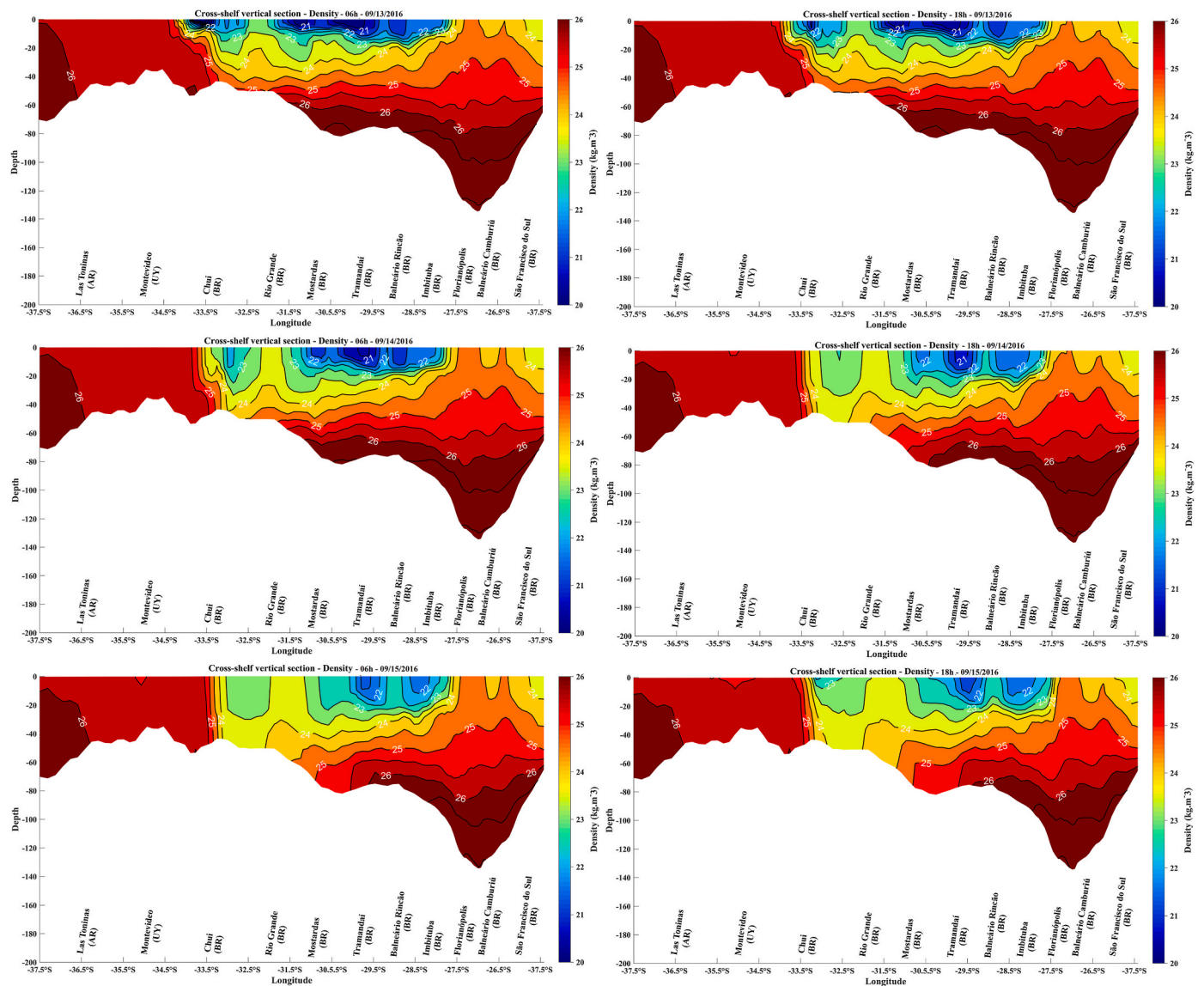


Fig. 9. Along continental shelf vertical profiles (~ 50 nautical miles offshore). Latitudinal vertical density from Las Toninas (AR) to São Francisco do Sul (BR). Density changes generated by coastal trapped wave propagation timeframes (letters a to f represent the extra-tropical cyclone temporal evolution). Units are sigma-theta.

During the wave propagation, we analyzed the depth-integrated momentum terms: acceleration (*accel*), horizontal and vertical advection (*hadv* - *vadv*), Coriolis force (*cor*), pressure gradient (*prsgrd*), horizontal and vertical viscosity (*hvisc* - *vvisc*). In Fig. 12a, the zonal acceleration term is strongly associated with the wave passage, with an amplitude greater than $2.10^{-5} \text{ m.s}^{-2}$. The Coriolis term follows the geostrophic flow induced by the wave crest, with values greater than 4.2 m.s^{-2} and a correlation coefficient of 0.82 between the pressure gradient and friction terms. The trapped wave reverses the pressure gradient and the over-shelf flow with a negative geostrophic flow (average westward shelf flow). The spatial dispersion average shows that the principal terms change with the growth pattern shown by the pressure gradient over time. The vertical, horizontal, and advective viscosity coefficients do not show significant correlations. The dynamic balance between velocity and pressure gradient primarily acts on the frictional and Ekman transport terms, with correlation coefficients greater than 0.61. In Fig. 12b, we observed the meridional component terms of the momentum equation, in which the northward propagation and the mean level rise due to the trapped wave passage induce a positive pressure gradient ($0.5.10^{-5} \text{ m s}^{-2}$) between 09/13 and 09/15. North of

Florianópolis, the negative sea level gradient creates a geostrophic flow ($-0.5.10^{-5} \text{ m s}^{-2}$), and the meridional acceleration term is strongly associated with upwelling/downwelling changes. The SBCS is not affected by the BC system, so the acceleration and Coriolis terms are influenced by the wave. So, its principal components govern the local hydrodynamic processes. The wave meridional component influences the horizontal turbulent viscosity term, which may explain the meridional density changes described in Fig. 9. The geostrophic approximation, through the pressure gradient, shows average values close to the acceleration and the Coriolis terms.

The heat transport through the north, south, and east boundaries of Rio Grande do Sul and Santa Catarina continental shelves is shown in Fig. 13. Negative (positive) values indicate a heat input (output) and a consequent heat gain (loss) from the coastal box. However, due to our short sampling period, it was not possible to perform correlations with other studies since previous works used monthly or seasonal surface heat averages. During September 11 and 13, the atmosphere was under a pre-frontal condition with the influence of the South Atlantic Subtropical High (SASH) and N-NE winds of up to 4 m s^{-1} . The STSW waters were transported into the box and later removed through the southern

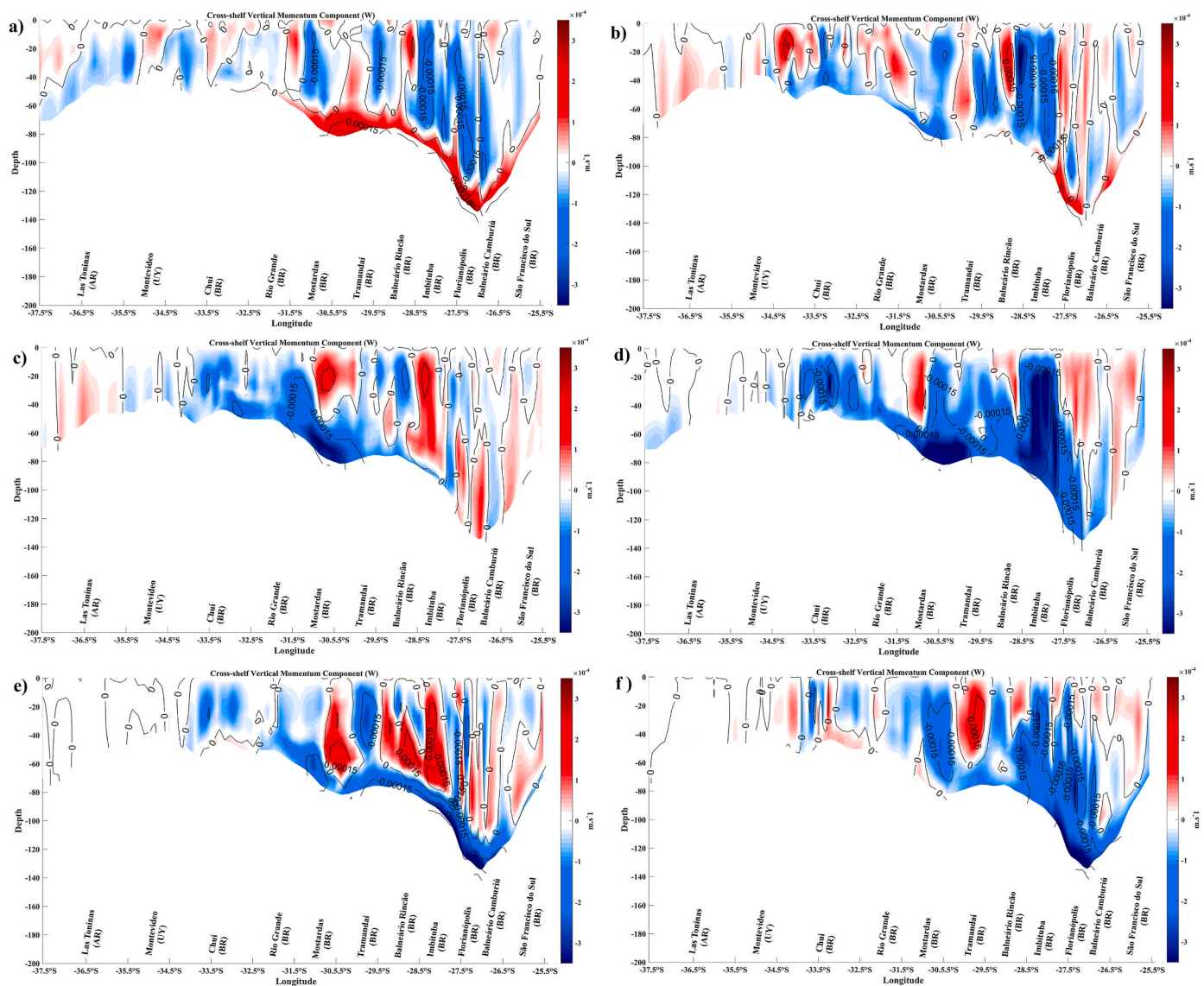


Fig. 10. Along continental shelf vertical profiles (~50 nautical miles offshore). Vertical velocity from Las Toninas (AR) to São Francisco do Sul (BR). Vertical changes generated by coastal trapped wave propagation timeframes (letters a to f represent the extra-tropical cyclone temporal evolution).

boundaries. The entrance of these relatively warm and salty waters and the absorbed heat from the atmosphere induced the total heat increase inside the model domain. The current and Ekman transport partially absorbed this energy and later advected it to the south. According to Tilburg & Gatvine [2004], the surface and bottom boundary layers interact at shallow depths on a shallow continental shelf such as the SBCS, whose slope is relatively smooth. This prevents the full development of a surface boundary layer and decreases the transport perpendicular to the wind stress. This turbulent process intensifies mixing and nutrient exchanges in the water column. Observing the correlation between the wind change and the mass and heat transport through the model’s coastal domain is possible. With the intensification of the extra-tropical cyclone on the southern coast of RS on September 14, there was a gradual inversion in the wind direction from the northwest (NW) to S-SW. September 14 to 16, the transport was northward, and there was a heat input through the east wall associated with Ekman transport. The change in the transport direction allowed colder waters to decrease the total heat in the coastal domain. It should be highlighted that these colder waters were not the SASW, but the STSW with approximately $-2\text{ }^{\circ}\text{C}$ of temperature, which is still within the thermohaline limit ($T > 14\text{ }^{\circ}\text{C}$ and $33.5 < S < 35.3$) described by Möller et al. [2008]. On

September 15, the south quadrant winds intensified, increasing the surface stress and reversing the transport, which reached the north wall of the coastal box with $\sim 0.6\text{ Sv}$. According to Schauer et al. [2004], in the case of a volume flow change, the mass must be balanced by altering the flow through the grid boundaries. This process is best observed in Fig. 13, where the total heat content decreased to $\sim 0.15 \times 10^{12}\text{ W}$ in only 36 h of activity of the synoptic system. On September 16–18, the wind direction changed to the N-NE, which consequently changed the oceanic heat transport (reductions of $\sim 0.1 \times 10^{12}\text{ W}$) to the south and the entrance of warm waters through the north wall of the model domain. However, since the cyclone moved away to the southeast grid and the N-NE winds returned, the heat transport followed the volume transport to the south. The gradual increase in the mass transport and heat flux to the south resulted from the horizontal advection of energy excess, observed on the first three days of simulation and between September 16 and 18. Decreasing heat values from September 14 to 16 indicated a gradual cooling process by horizontal advection, which was directly associated with the transport through the grid south boundary.

Our work, as well as De Freitas et al. (2021), wants to show that waves pressing on the SBCS are common during the year, and their width variation alters the acceleration of the wave propagation.

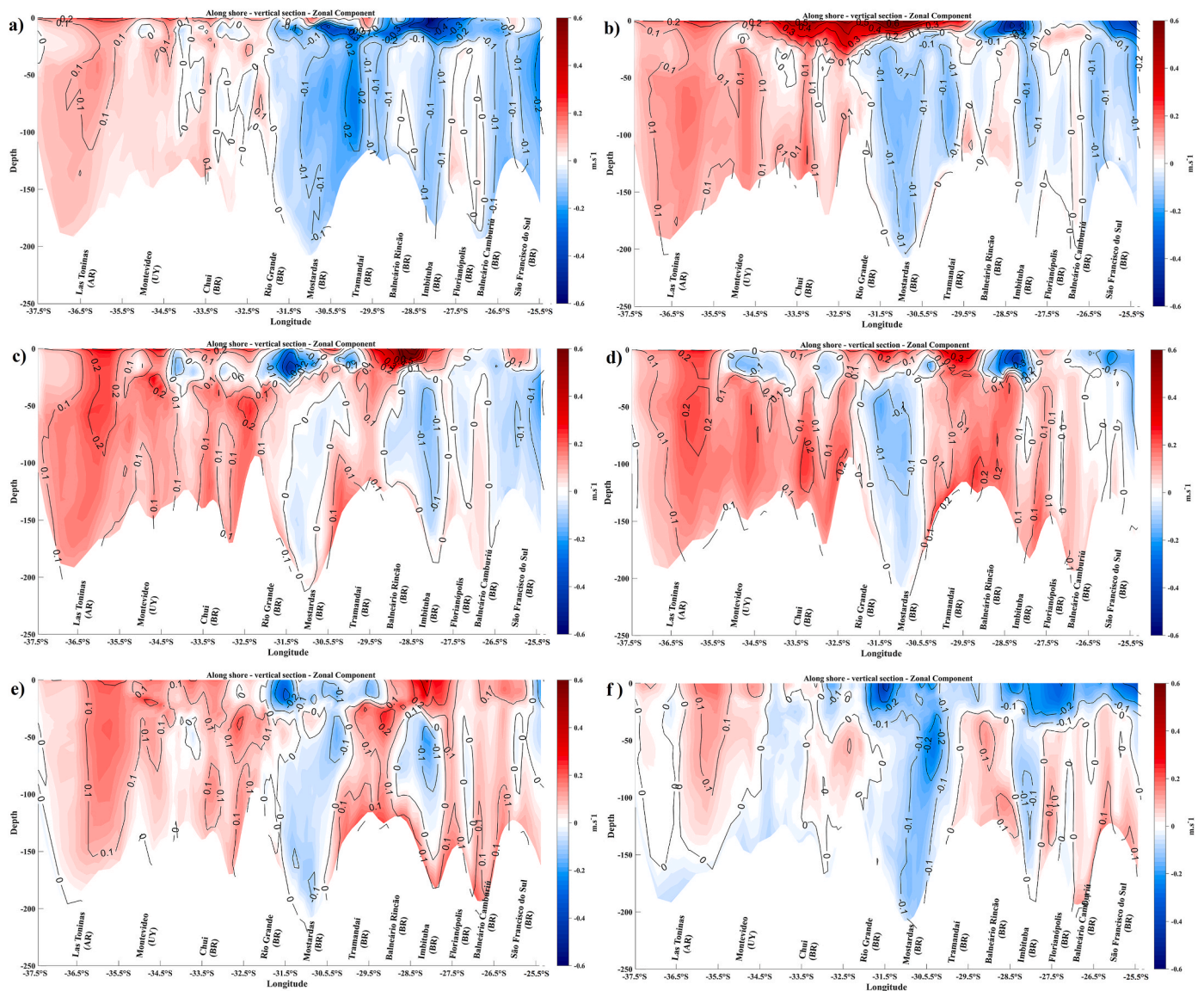


Fig. 11. Along continental shelf vertical profiles (~ 50 nautical miles offshore). Zonal velocity from Las Toninas (AR) to São Francisco do Sul (BR). U-component (East-West) changes generated by coastal trapped wave propagation timeframes (letters a to f represent the extra-tropical cyclone temporal evolution).

Seasonal stratification creates a barotropic response to wind disturbances. According to Möller et al. (2008) and Piola et al. (2008), the local wind changes the current speeds and transport along the SBCS. Costa and Möller (2011) and Andrade et al. (2016) used data from acoustic profilers to show that the current's direction on the SBCS oppositely changes throughout the water column a few hours after the wind change. Dias et al. (2014) added that it is not only the offshore Ekman transport responsible for the physical-chemical changes on the SBCS, but the coastline geometry is also important. Our results show that crossing an intense atmospheric system can modify the local hydrodynamic conditions, especially in shallow waters driven by winds. Rodrigues et al. (2004) showed that cold fronts move on the SBCS from southeast to northeast with a monthly frequency of 3–4 fronts/month, usually followed by mobile cyclones and anticyclones. Therefore, the changes generated by these synoptic systems directly influence the thermohaline structure and the coastal waters' oxygenation.

4. Conclusions

In an unprecedented way, this work uses a coupled ocean-atmospheric model to investigate the September 2016 hydrodynamical

consequences of an extra-tropical cyclone-induced trapped coastal wave propagating over the SBCS. Model solutions use boundary components adjusted for the local conditions from an earlier study (Mendonça et al., 2017), and the results demonstrate a regional circulation pattern strongly associated with an active meteorological system in the southern Brazilian region (correlation values greater than 78%). These processes change the physical and chemical seawater properties by changing the mixing layer and fertilizing the shelf waters. The generation area of these waves extends from the Patagonian shelf to southern Brazil. The SBCS is not affected by the BC system, so the acceleration and Coriolis terms are influenced by the wave. So, its principal components govern the local hydrodynamic processes. The wave meridional component influences the horizontal turbulent viscosity term, which may explain the meridional density changes. This trapped wave changes amplitude and velocity according to the shelf width and generates a barotropic gradient that enhances the zonal exchanges between the shelf and offshore areas. In addition, it will modify the mixing and bottom layer, enabling vertical migration of organisms and nutrients. The analyzed period consisted of the rapid formation of an extra-tropical cyclone, intensifying the south-quadrant winds and the associated Ekman transport. Despite the fast change in pressure fields, we did not observe

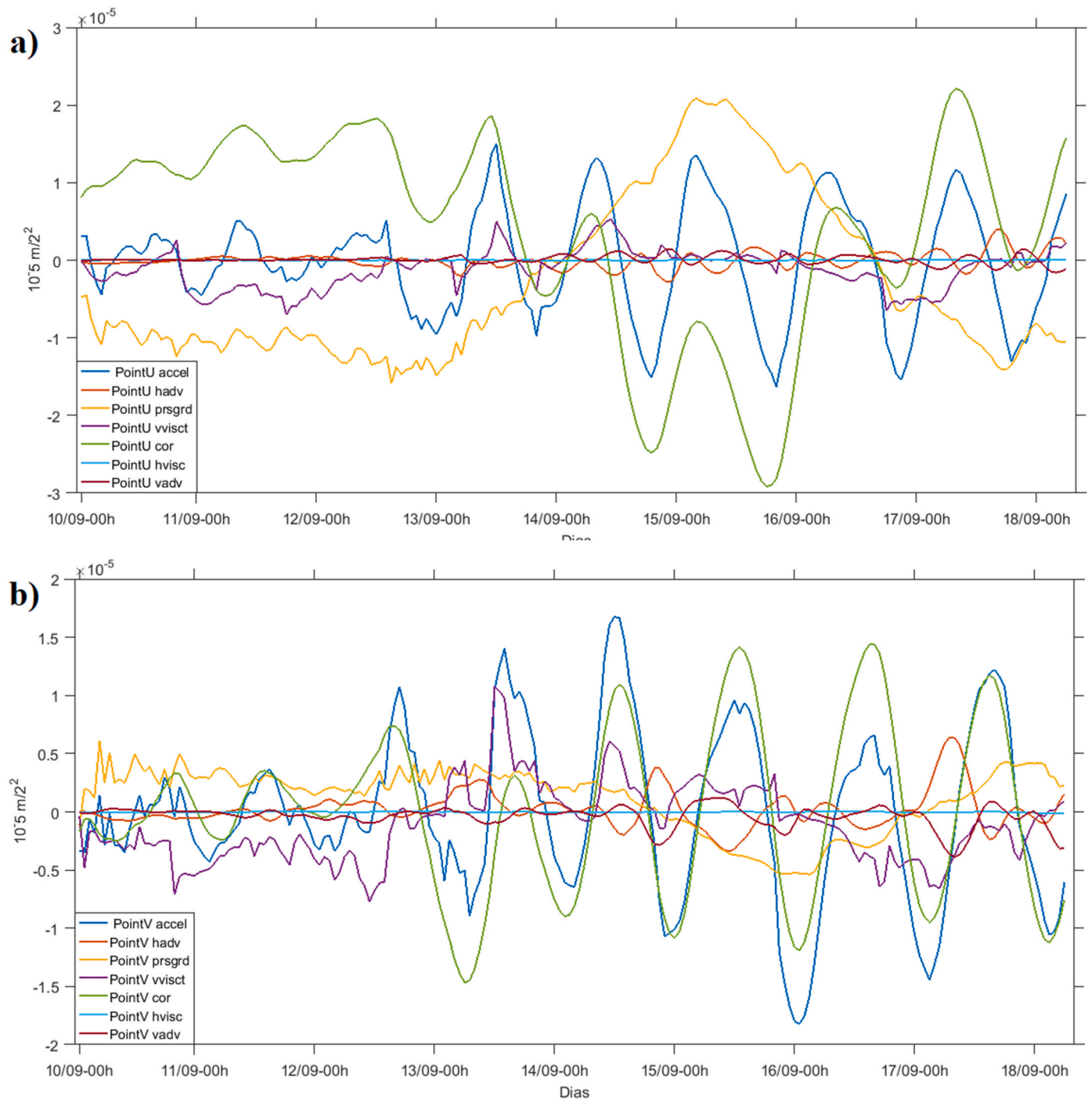


Fig. 12. Time series of the model momentum balance terms calculated in the along-shelf in $\text{m}\cdot\text{s}^{-1}$. Along-shelf velocities are represented by acceleration (*accel*). Frictional terms are represented by vertical viscosity (*hvisc* - *vvisc*) and horizontal and vertical advection (*hadv* - *vadv*). Along-shelf pressure gradient (*prsgrd*). Ekman drifts are represented by Coriolis force (*cor*).

the inverted barometer effect, and the upwelling on the Uruguayan coast was caused exclusively by surface wind drag. Filtering the model altimetric data allowed the identification of the low-frequency storm surge component with a low lag in relation to the tidal gauge. This process was essential, allowing a coastal wave analysis intensified by the frontal system winds responsible for flooding several cities along the southern Brazilian coast.

Our manuscript shows that the crossing of trapped waves, generated by extra-tropical cyclones, changes the hydrodynamic local conditions of the southern Brazilian continental shelf. The heat transporting through the southern, northern, and eastern boundaries influences the

exchanges between shelf-offshore and ocean-atmosphere, in addition to fertilizing the continental shelf with nutrients to create specific conditions developing phyto and zooplankton species. Although the relationship between wind forcing, wave, and the resulting flux is not linear, the correlation coefficient gives us a measure of wave propagation behavior on the continental shelf. A qualitative assessment delineated the conditions for the development of large waves trapped on the coast associated with tropical cyclones: when the storm moves for several hours, its translation speed slowly increases, continuously matching the group velocity of the waves under the storm. The strong correlation between winds and shelf currents at the surface and on the bottom shows

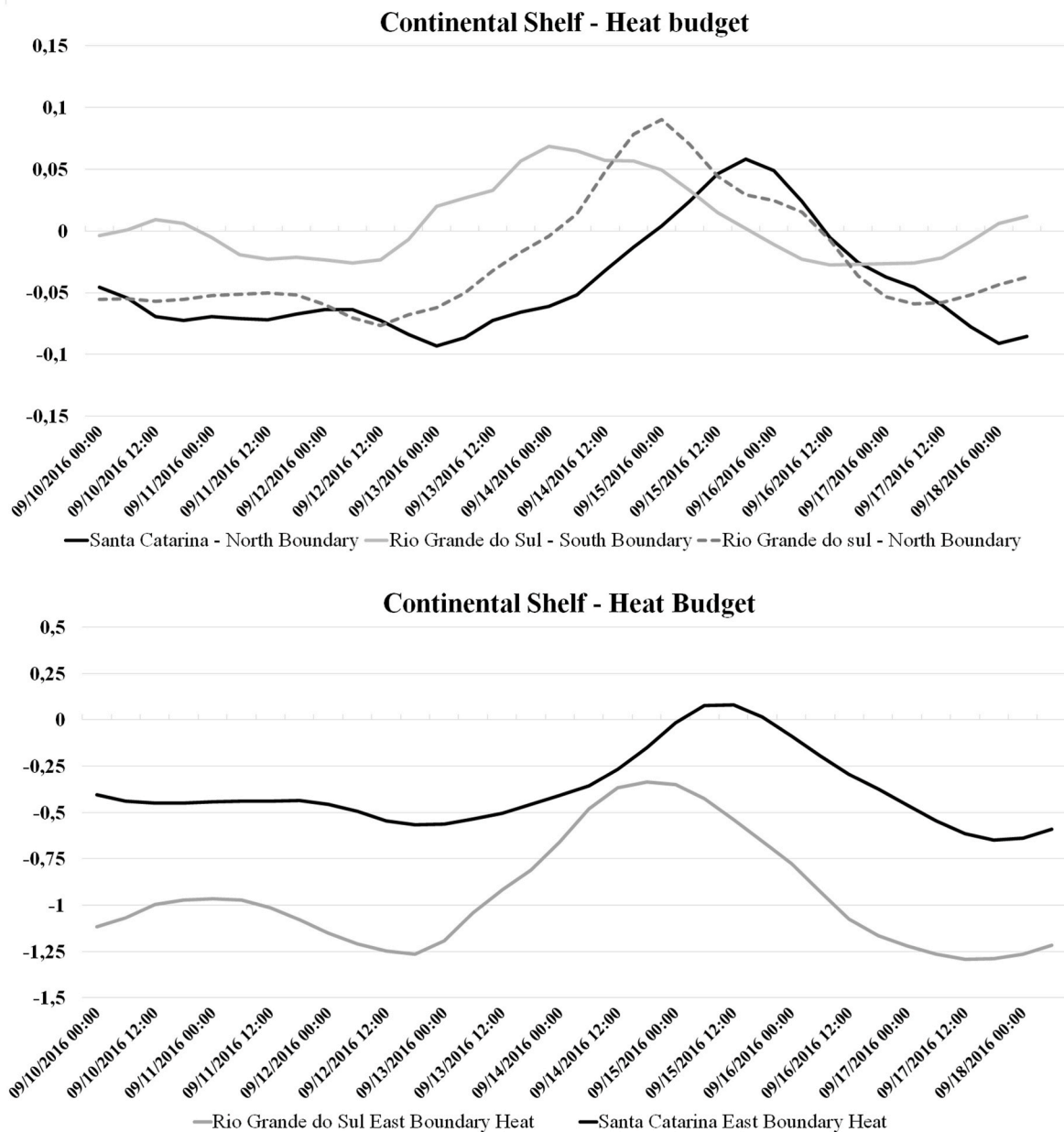


Fig. 13. Heat Budget (in TW) calculated for the Rio Grande do Sul and Santa Catarina Continental Shelves during the coastal trapped wave crossing.

a rapid response to wind forcing. Since the southern region of Brazil is constantly affected by the crossing of frontal systems, studies capable of interpreting the changes in the SBCS dynamics have great importance for the ecological characterization and the prevention of coastal impacts associated with sea level variations.

CRedit authorship contribution statement

Luis Felipe Ferreira de Mendonça: Writing – review & editing, Writing – original draft, Visualization, Validation, Supervision, Software, Resources, Project administration, Methodology, Investigation, Funding acquisition, Formal analysis, Data curation, Conceptualization. **Antônio Fernando Harter Fetter Filho:** Writing – review & editing, Writing – original draft, Visualization, Supervision, Conceptualization. **Mauro Michelena Andrade:** Writing – review & editing, Writing – original draft, Methodology, Data curation. **Fabricio Sanguinetti Cruz de Oliveira:** Writing – review & editing, Writing – original draft, Methodology. **Douglas da Silva Lindemann:** Writing – review &

editing, Writing – original draft, Methodology. **Rose Ane Pereira de Freitas:** Writing – review & editing, Writing – original draft, Methodology. **Rafael Afonso do Nascimento Reis:** Writing – review & editing, Writing – original draft, Methodology, Data curation. **Carlos Alexandre Domingos Lentini:** Writing – review & editing, Writing – original draft. **Claudia Klose Parise:** Writing – review & editing, Investigation, Formal analysis. **Daniel Caetano Santos:** Validation, Methodology, Data curation.

Declaration of competing interest

The authors declare the following financial interests/personal relationships which may be considered as potential competing interests: PhD Luis Felipe Ferreira de Mendonca reports financial support and administrative support were provided by National Council for Scientific and Technological Development.

Data availability

Data will be made available on request.

Acknowledgments

We thank CNPq and INCT-Mar COI for funding in the form of a postdoctoral fellowship. As faculty members, LFFM and CADL would like to thank the Graduate Program in Geophysics (PPGEOFISICA) at the Federal University of Bahia. This research also was received funding from the European Union's Horizon 2020 Research and Innovation Program under grant agreement (Call H2020-BG-2018-2020) No 862923. This output reflects only the author's view, and the European Union cannot be held responsible for any use that may be made of the information contained therein. We thank the Agricultural Research and Rural Extension Company of Santa Catarina (EPAGRI), which provided free of charge the tide data and Dr. Elirio Ernestino Toldo Junior (Federal University of Rio Grande do Sul) for the sea level data provided together with Prof. Dr. Mauro Michelena Andrade (Univali).

References

- Alcaraz, M., Marrasé, C., Peters, F., Arin, L., Malits, A., 2002. Effects of turbulence conditions on the balance between production and respiration in marine planktonic communities. *Mar. Ecol.: Prog. Ser.* 242, 63–71.
- Amante, C., Eakins, B.W., 2009. ETOPO1 1 Arc-Minute Global Relief Model: Procedures, Data Sources and Analysis. National Geophysical Data Center, NOAA. <https://doi.org/10.7289/V5C8276M>. NOAA Technical Memorandum NESDIS NGDC-24.
- Ambrizzi, T., Souza, E.B., Pulwarty, R.S., 2004. The Hadley and Walker regional circulations and associated ENSO impacts on the South American seasonal rainfall. In: Diaz, Henry F., Bradley, Raymond S. (Eds.), *The Hadley Circulation: Present, Past and Future*, 1 ed., vol. 21. Kluwer Academic Publishers, Netherlands, pp. 203–235 (Org.).
- Andrade, M.M., Toldo Jr., E., Nunes, J.C., 2016. Variability of currents on the inner shelf of Tramandaí (RS) during the summer of 2014. *Geosci. Res.* 43 (4), 289–298.
- Andrade, M.M., Toldo, E.E., Nunes, J.C.R., 2018. Tidal and subtidal oscillations in a shallow water system in southern Brazil. *Braz. J. Oceanogr.* 66 (3), 245–254.
- Babanin, A.V., 2006. On a wave-induced turbulence and a wave-mixed upper ocean layer. *Geophys. Res. Lett.* 33 (20).
- Battisti, D.S., Hickey, B.M., 1984. Application of remote wind-forced coastal trapped wave theory to the Oregon and Washington coasts. *J. Phys. Oceanogr.* 14 (5), 887–903.
- Bender, M.A., Ginis, I., Kurihara, Y., 1993. Numerical simulations of tropical cyclone-ocean interaction with a high-resolution coupled model. *J. Geophys. Res. Atmos.* 98 (D12), 23245–23263.
- Bitencourt, D.P., Manoel, G., Acevedo, O.C., Fuentes, M.V., Muza, M.N., Rodrigues, M.L., Leal Quadro, M.F., 2011. Relating winds along the Southern Brazilian coast to extratropical cyclones. *Meteorol. Appl.* 18 (2), 223–229.
- Brink, K.H., 1991. Coastal-trapped waves and wind-driven currents over the continental shelf. *Annu. Rev. Fluid Mech.* 23 (1), 389–412.
- Bubalo, M., Janeković, I., Orlić, M., 2018. Chrystal and Proudman resonances simulated with three numerical models. *Ocean Dynam.* 68, 497–507.
- Calliari, L.J., Tozzi, H.A.M., Klein, A.H.F., 1988. Beach morphology and coastline erosion associated with storm surge in Southern Brazil-Rio Grande to Chuí, RS. *Annals of the Brazilian Academy of Science* 70 (2).
- Camargo, R., Tódesco, E., Pezzi, L.P., Souza, R.B., 2013. Modulation mechanisms of marine atmospheric boundary layer at the Brazil-Malvinas Confluence region. *J. Geophys. Res. Atmos.* 118 (12), 6266–6280.
- Camayo, R., Campos, E.J., 2006. Application of wavelet transform in the study of coastal trapped waves off the west coast of South America. *Geophys. Res. Lett.* 33 (22).
- Campos, E.J.D., Gonçalves, J.E., Ikeda, Y., 1995. Water mass characteristics and geostrophic circulation in the South Brazil Bight: summer of 1991. *J. Geophys. Res.* 100 (C9), 18537–18550. <https://doi.org/10.1029/95JC01724>.
- Carvajal, M., Contreras-López, M., Winckler, P., Sepúlveda, I., 2017. Meteotsunamis occurring along the southwest coast of South America during an intense storm. *Pure Appl. Geophys.* 174, 3313–3323.
- Casagrande, L., Tomasella, J., dos Santos Alvalá, R.C., 2017. Early flood warning in the Itajaí-Açu River basin using numerical weather forecasting and hydrological modeling. *Nat. Hazards* 88, 741–757. <https://doi.org/10.1007/s11069-017-2889-0>.
- Casey, K.S., Brandon, T.B., Cornillon, P., Evans, R., 2010. The past, present, and future of the AVHRR Pathfinder SST program. In: *Oceanography from Space*. Springer, Netherlands, pp. 273–287.
- Castro, B., Lee, T., 1995. Wind-forced sea level variability on the southeast Brazilian shelf. *J. Geophys. Res.* 100, 16045–16056.
- Cocke, S., Larow, T.E., 2000. Seasonal predictions using a regional spectral model embedded within a coupled ocean-atmosphere model. *Mon. Weather Rev.* 128 (3), 689–708.
- Costa, R., Möller, O.O., 2011. Study of the structure and variability of currents in the area of the inner shelf off Rio Grande (RS, Brazil), southwest of the South Atlantic during spring-summer 2006-2007. *Journal of Integrated Coastal Zone Management* 11 (3), 273–281.
- Dal Piva, E., Gan, M.A., de Lima Moscatti, M.C., 2011. The role of latent and sensible heat fluxes in an explosive cyclogenesis over the South American East Coast. *Journal of the Meteorological Society of Japan. Ser. II* 89 (6), 637–663.
- De Freitas, P.P., de Moraes Paiva, A., Cirano, M., Mill, G.N., da Costa, V.S., Gabioux, M., França, B.R.L., 2021. Coastal trapped waves propagation along the southwestern Atlantic continental shelf. *Contin. Shelf Res.* 226, 104496.
- Dean, R.G., Dalrymple, R.A., 1991. *Water Wave Mechanics for Engineers and Scientists*, vol. 2. World scientific, Singapore, p. 353.
- Dias, D.F., Pezzi, L.P., Gherardi, D.F.M., Camargo, R., 2014. Modeling the spawning strategies and larval survival of the Brazilian sardine (*Sardinella brasiliensis*). *Prog. Oceanogr.* 123, 38–53.
- Diaz, A.F., Studzinski, C.D., Mechoso, C.R., 1998. Relationships between precipitation anomalies in Uruguay and Southern Brazil and sea surface temperature in the Pacific and Atlantic Oceans. *J. Clim.* 11, 251–271.
- Do Vale Silva, T.L., Veleda, D., Araujo, M., Tyaquicã, P., 2018. Ocean-atmosphere feedback during extreme rainfall events in eastern northeast Brazil. *J. Appl. Meteorol. Climatol.* 57 (5), 1211–1229.
- Domps, B., Marmain, J., Guérin, C.A., 2021. A reanalysis of the October 2016 “Meteotsunami” in British Columbia with help of high-frequency radars and autoregressive modeling. *Geosci. Rem. Sens. Lett. IEEE* 19, 1–5.
- Dottori, M., Castro, B.M., 2018. The role of remote wind forcing in the subinertial current variability in the central and northern parts of the South Brazil Bight. *Ocean Dynam.* 68, 677–688. <https://doi.org/10.1007/s10236-018-1153-9>.
- Dudhia, J., 1989. Numerical study of convection observed during the Winter Monsoon Experiment using a mesoscale two-dimensional model. *J. Atmos. Sci.* 46, 3077–3107. [https://doi.org/10.1175/1520-0469\(1989\)046<3077:NSOCOD>2.0.CO;2](https://doi.org/10.1175/1520-0469(1989)046<3077:NSOCOD>2.0.CO;2)PDF.
- Echevin, V., Albert, A., Lévy, M., Graco, M., Aumont, O., Piétri, A., Garric, G., 2014. Intraseasonal variability of nearshore productivity in the Northern Humboldt Current System: the role of coastal trapped waves. *Contin. Shelf Res.* 73, 14–30.
- Egbert, G.D., Erofeeva, S.Y., 2010. The Osu Topex/poseidon Global Inverse Solution Tpxo. Oregon State University.
- Escobar, G.C., Seluchi, M.E., Andrade, K., 2016. Synoptic classification of cold fronts associated with extremes rainfall over the east of Santa Catarina state. *Brazilian Journal of Meteorology* 31 (4), 649–661.
- Fandry, c.B., 1984. Development of numerical model of tidal and wind-driven circulation in Bass Strait. *Aust. J. Mar. Freshw. Res.* 32, 9–29.
- Fetter, A.F.H., Matano, R.P., 2008. On the origins of the variability of the Malvinas Current in a global, eddy-permitting, numerical simulation. *J. Geophys. Res.* 113, C11018 <https://doi.org/10.1029/2008jc004875>.
- Filippo, A., Kjerfve, B., Torres Júnior, A.R., Fernandes, A.M., 2012. Low-frequency variability of sea level along the mid-atlantic coast of south America. *Braz. J. Genet.* 30, 5–14. <https://doi.org/10.22564/rbgfv30i1.64>.
- Gan, M.A., Rao, V.B., 1991. Surface cyclogenesis over South America. *Mon. Weather Rev.* 119 (5), 1293–1302.
- Gibbs, J.A., Fedorovich, E., Van Eijk, A.M., 2011. Evaluating Weather Research and Forecasting (WRF) model predictions of turbulent flow parameters in a dry convective boundary layer. *J. Appl. Meteorol. Climatol.* 50 (12), 2429–2444.
- Gill, A.E., 1982. Atmosphere-Ocean Dynamics International Geophysics Series 30, 662.
- Gill, A.E., Clarke, A.J., 1974. Wind-induced upwelling, coastal currents and sea-level changes. In: *Deep Sea Research and Oceanographic Abstracts*, vol. 21. Elsevier, pp. 325–345, 5.
- Gozzo, L.F., Da Rocha, R.P., 2013. Air-sea interaction processes influencing the development of a Shapiro-Keyser type cyclone over the subtropical South Atlantic Ocean. *Pure Appl. Geophys.* 170 (5), 917–934.
- Gozzo, L.F., da Rocha, R.P., Reboita, M.S., Sugahara, S., 2014. Subtropical cyclones over the southwestern South Atlantic: climatological aspects and case study. *J. Clim.* 27 (22), 8543–8562.
- Gramscianinov, C.B., Hodges, K.I., Camargo, R., 2019. The properties and genesis environments of South Atlantic cyclones. *Clim. Dynam.* 53 (7–8), 4115–4140.
- Green, M.O., Coco, G., 2014. Review of wave-driven sediment resuspension and transport in estuaries. *Rev. Geophys.* 52 (1), 77–117.
- Gronholz, A., Gräwe, U., Paul, A., Schulz, M., 2017. Investigating the effects of a summer storm on the North Sea stratification using a regional coupled ocean-atmosphere model. *Ocean Dynam.* 67 (2), 211–235.
- Guimarães, P.V., Farina, L., Toldo Jr., E.E., 2014. Analysis of extreme wave events on the southern coast of Brazil. *Nat. Hazards Earth Syst. Sci.* 14 (12), 3195–3205.
- Haidvogel, D.B., Arango, H.G., Hedstrom, K., Beckmann, A., Malanotte-Rizzoli, P., Schchepetkin, A.F., 2000. Model evaluation experiments in the North Atlantic Basin: simulations in nonlinear terrain-following coordinates. *Dynam. Atmos. Oceans* 32, 239–281.
- Hermes, J.C., Reason, C.J.C., 2005. Ocean model diagnosis of interannual coevolving SST variability in the South Indian and South Atlantic Oceans. *J. Clim.* 18 (15), 2864–2882.
- Hoeke, R.K., McInnes, K.L., Kruger, J.C., McNaught, R.J., Hunter, J.R., Smithers, S.G., 2013. Widespread inundation of Pacific islands triggered by distant-source wind-waves. *Global Planet. Change* 108, 128–138.
- Hong, S.Y., Dudhia, J., Chen, S.H., 2004. A revised approach to ice microphysical processes for the bulk parameterization of clouds and precipitation. *Mon. Weather Rev.* 132 (1), 103–120.
- Hong, S.Y., Noh, Y., Dudhia, J., 2006. A new vertical diffusion package with an explicit treatment of entrainment processes. *Mon. Weather Rev.* 134 (9), 2318–2341. <https://doi.org/10.1175/Mwr3199.1>.

- Hoskins, B.J., Hodges, K.I., 2005. A new perspective on southern hemisphere storm tracks. *J. Clim.* 18 (20), 4108–4129.
- Houghton, R.W., Beer, T., 1976. Wave propagation during the Ghana upwelling. *J. Geophys. Res.* 81 (24), 4423–4429.
- Illig, S., Bachélery, M.L., Cadier, E., 2018. Subseasonal coastal-trapped wave propagations in the southeastern Pacific and Atlantic Oceans: 2. Wave characteristics and connection with the equatorial variability. *J. Geophys. Res.: Oceans* 123 (6), 3942–3961.
- Innocentini, V., Caetano Neto, E., 1996. A case study of the 9 August 1998 south atlantic storm: numerical simulations of the wave activity. *Weather Forecast.* 11, 78–88.
- Junker, T., Mohrholz, V., Schmidt, M., Siegfried, L., van der Plas, A., 2019. Coastal trapped wave propagation along the southwest African shelf as revealed by moored observations. *J. Phys. Oceanogr.* 49 (3), 851–866.
- Kain, John S., 2004. The Kain–Fritsch convective parameterization: an update. *J. Appl. Meteorol.* 43, 170–181. [https://doi.org/10.1175/1520-0450\(2004\)043<0170:TKCPAU>2.0.CO;2](https://doi.org/10.1175/1520-0450(2004)043<0170:TKCPAU>2.0.CO;2)PDF.
- Kantha, L.H., Clayson, C.A., 2000. Numerical models of oceans and oceanic processes. In: *International Geophysics Series*, vol. 66. Academic Press, p. 940. Foreword by Kirk Bryan.
- Kitade, Y., Matsuyama, M., 2000. Coastal-trapped waves with several-day period caused by wind along the southeast coast of Honshu, Japan. *J. Oceanogr.* 56 (6), 727–744.
- Kleczeck, M.A., Steeneveld, G.J., Holtslag, A.A., 2014. Evaluation of the weather research and forecasting mesoscale model 4 for GABLS3: impact of boundary-layer schemes, boundary conditions and spin-up. *Boundary-layer meteorol.* 152 (2), 5 213–243.
- Krüger, L.F., da Rocha, R.P., Reboita, M.S., Ambrizzi, T., 2012. RegCM3 nested in HadAM3 scenarios A2 and B2: projected changes in extratropical cyclogenesis, temperature and precipitation over the South Atlantic Ocean. *Climatic Change* 113, 599–621.
- Lee, D.E., Kim, J., Heo, Y., Kang, H., Lee, E.Y., 2021. Climate change implications found in winter extreme sea level height records around Korea. *J. Mar. Sci. Eng.* 9 (4), 377.
- Lima, I., Castello, J.P., 1995. Distribution and abundance of Southwest Atlantic anchovy spawners (*Engraulis anchoita*) in relation to oceanographic processes on the southern Brazilian shelf. *Fish. Oceanogr.* 4 (1), 1–16.
- Lionello, P., Conte, D., Reale, M., 2019. The effect of cyclones crossing the Mediterranean region on sea level anomalies on the Mediterranean Sea coast. *Nat. Hazards Earth Syst. Sci.* 19 (7), 1541–1564.
- Machado, J.P., Justino, F., Souza, C.D., 2020. Influence of El Niño-southern oscillation on baroclinic instability and storm tracks in the southern hemisphere. *Int. J. Climatol.* <https://doi.org/10.1002/joc.6651>.
- Matano, R.P., Palma, E.D., Piola, A.R., 2010. The influence of the Brazil and Malvinas currents on the southwestern Atlantic shelf circulation. *Ocean Sci.* 6, 983–995.
- Matano, R.P., Combes, V., Piola, A.R., Guerrero, R., Palma, E.D., Strub, P.T., James, C., Fenco, H., Chao, Y., Saraceno, M., 2014. The salinity signature of the cross-shelf exchanges in the southwestern Atlantic Ocean: numerical simulations. *J. Geophys. Res. Oceans* 119, 7949–7968. <https://doi.org/10.1002/2014JC010116>.
- Melo, E., Romeu, M.A.R., Hammes, G.R., 2008. Reconstruction of sea state conditions at the Vitoria and Santa Catarina coasts (Brazil during the June 2006 swell event). In: *7th International Conference on Coastal and Port Engineering in Developing Countries*, Dubai, pp. 1–15.
- Mendonça, L.F.F., Souza, R.B., Aseff, C.R.C., Pezzi, L.P., Möller, O.O., Alves, R.C., 2017. Regional modeling of the water masses and circulation annual variability at the Southern Brazilian Continental Shelf. *Journal of Geophysical Research, Oceans* 121, 1010022016JC011780.
- Meza-Padilla, R., Appendini, C.M., Pedrozo-Acuña, A., 2015. Hurricane-induced waves and storm surge modeling for the Mexican coast. *Ocean Dynam.* 65 (8), 1199–1211.
- Mlawer, Eli, J., Steven, J.T., Patrick, D.B., Iacono, M.J., Clough, S.A., 1997. Radiative transfer for inhomogeneous atmospheres: RRTM, a validated correlated- k model for the longwave. *J. Geophys. Res. B* 102, 16663–16682. <https://doi.org/10.1029/97JD00237PDF>.
- Möller, O.O., Piola, A.R., Freitas, A.C., Campos, E.J.D., 2008. The effects of river discharge and seasonal winds on the shelf off southeastern South America. *Continent. Shelf Res.* 28, 1607–1624.
- Musgrave, R.C., 2019. Energy fluxes in coastal trapped waves. *J. Phys. Oceanogr.* 49 (12), 3061–3068.
- Niu, Guo-Yue, Zong-Liang, Y., Kenneth, E.M., Fei, C., Michael, B.E., Michael, B., Anil, K., Kevin, M., Dev, N., Enrique, R., M, T., Youlong, X., 2011. The community Noah land surface model with multiparameterization options (Noah-MP): 1. Model description and evaluation with local-scale measurements. *J. Geophys. Res.* 116, D12109 <https://doi.org/10.1029/2010JD015139>.
- Palma, E.D., Matano, R.P., 2009. Disentangling the upwelling mechanisms of the South Brazil bight. *Continent. Shelf Res.* 29, 1525–1534.
- Palma, E.D., Matano, R.P., Piola, A.R., 2004. A numerical study of the Southwestern Atlantic Shelf circulation: barotropic response to tidal and wind forcing. *J. Geophys. Res.* 109, C08014.
- Palma, E.D., Matano, R.P., Piola, A.R., 2008. A numerical study of the Southwestern Atlantic Shelf circulation: stratified ocean response to local and offshore forcing. *J. Geophys. Res.* 113 (C11), C111010.
- Parise, C.K., Calliari, L.J., Krusche, N., 2009. Extreme storm surges in the south of Brazil: atmospheric conditions and shore erosion. *Braz. J. Oceanogr.* 57 (3), 175–188. <https://doi.org/10.1590/S1679-87592009000300002>.
- Perlin, N., Skyllingstad, E.D., Samelson, R.M., 2011. Coastal atmospheric circulation around an idealized cape during wind-driven upwelling studied from a coupled ocean-atmosphere model. *Mon. Weather Rev.* 139 (3), 809–829.
- Pietri, A., Echevin, V., Testor, P., Chaigneau, A., Mortier, L., Grados, C., Albert, A., 2014. Impact of a coastal-trapped wave on the near-coastal circulation of the Peru upwelling system from glider data. *J. Geophys. Res.: Oceans* 119 (3), 2109–2120.
- Piola, A.R., Campos, E.J.D., Möller Jr., O.O., Charo, M., Martinez, C., 2000. Subtropical shelf front off eastern South America. *J. Geophys. Res.* 105 (C3), 6565–6578.
- Piola, A.R., Möller Jr., O.O., Guerrero, R.A., Campos, E.J.D., 2008. Variability of the Subtropical Shelf front off eastern South America: winter 2003 and summer 2004. *Continent. Shelf Res.* 28, 1639–1648.
- Piola, A.R., Martínez Avellaneda, N., Guerrero, R.A., Jardon, F.P., Palma, E.D., Romero, S.I., 2010. Malvinas-slope water intrusions on the northern Patagonia continental shelf. *Ocean Sci.* 6 (1), 345–359.
- Pizarro, O., Clarke, A.J., Van Gorder, S., 2001. El Niño sea level and currents along the South American coast: comparison of observations with theory. *J. Phys. Oceanogr.* 31 (7), 1891–1903.
- Pontes, R.M., Gaspar, P., 1999. Regional analysis of the inverted barometer effect over the global ocean using TOPEX/POSEIDON data and model results. *J. Geophys. Res.: Oceans* 104 (C7), 15587–15601.
- Powers, J.G., Klemp, J.B., Skamarock, W.C., Davis, C.A., Dudhia, J., Gill, D.O., Duda, M. G., 2017. The weather research and forecasting model: overview, system efforts, and future directions. *Bull. Am. Meteorol. Soc.* 98 (8), 1717–1737.
- Proudman, J., 1929. The effects on the sea of changes in atmospheric pressure. *Geophysical Supplements to the Monthly Notices of the Royal Astronomical Society* 2 (4), 197–209.
- Pugh, D.T., 1987. *Tides, Surges and Mean Sea Level: A Handbook for Engineers and Scientists*, vol. 472. John Wiley, New York.
- Rabinovich, A., Šepić, J., Thomson, R., 2022. The Extreme Sea-Level Event of 14–15 October 2016 on the Coasts of British Columbia and Washington State Caused by Typhoon “Songda” (No. EGU22-10966). *Copernicus Meetings*.
- Reale, M., Liberato, M.L., Lionello, P., Pinto, J.G., Salon, S., Ulbrich, S., 2019. A global climatology of explosive cyclones using a multi-tracking approach. *Tellus Dyn. Meteorol. Oceanogr.* 71 (1), 1611340.
- Reboita, M.S., da Rocha, R.P., Ambrizzi, T., Sugahara, S., 2010. South Atlantic Ocean cyclogenesis climatology simulated by regional climate model RegCM3. *Clim. Dynam.* 35 (7–8), 1331–1347.
- Reboita, M.S., Da Rocha, R.P., Oliveira, D.M.D., 2019. Key features and adverse weather of the named subtropical cyclones over the southwestern South Atlantic ocean. *Atmosphere* 10 (1), 6.
- Reboita, M.S., Reale, M., da Rocha, R.P., Giorgi, F., Giuliani, G., Coppola, E., Cavazos, T., 2020. Future Changes in the Wintertime Cyclonic Activity over the CORDEX-CORE Southern Hemisphere Domains in a Multi-Model Approach.
- Reynolds, R.W., Smith, T.M., Liu, C., Chelton, D.B., Casey, K.S., Schlax, M.G., 2007. Daily high-resolution-blended analyses for Sea Surface temperature. *J. Clim.* 20, 5473–5496.
- Rintoul, S.R., England, M.H., 2002. Ekman transport dominates local air–sea fluxes in driving variability of Subantarctic Mode Water. *J. Phys. Oceanogr.* 32 (5), 1308–1321.
- Rippeth, T.P., Palmer, M.R., Simpson, J.H., Fisher, N.R., Sharples, J., 2005. Thermocline mixing in summer stratified continental shelf seas. *Geophys. Res. Lett.* 32 (5).
- Rocha, R.P., Sugahara, S., Silveira, R.B., 2004. Sea waves generated by extratropical cyclones in the south Atlantic Ocean: hindcast and validation against altimeter data. *Weather Forecast.* 19, 398–410.
- Rocha, R.P., Reboita, M.S., Gozzo, L.F., Dutra, L.M.M., de Jesus, E.M., 2018. Subtropical cyclones over the oceanic basins: a review. *Ann. N. Y. Acad. Sci.* 1436 (1), 138–156.
- Rodrigues, M.L.G., Franco, D., Sugahara, S., 2004. Climatology of fronts in Santa Catarina coast. *Braz. J. Genet.* 22 (2), 135–151.
- Romea, R.D., Smith, R.L., 1983. Further evidence for coastal trapped waves along the Peru coast. *J. Phys. Oceanogr.* 13 (8), 1341–1356.
- Rosa, M.B., Ferreira, N.J., Gan, M.A., Machado, L.H.R., 2013. Energetics of cyclogenesis events over the southern coast of Brazil. *Revista Brasileira de Meteorologia* 28 (3), 231–245.
- Saldanha-Corrêa, F.M.P., Giancesella, S.M.F., 2004. A microcosm approach on the potential effects of the vertical mixing of water masses over the primary productivity and phytoplankton biomass in the southern Brazilian coastal region. *Braz. J. Oceanogr.* 52 (3–4), 167–182.
- Saraceno, M., Provost, C., Piola, A.R., 2005. On the relationship between satellite-retrieved surface temperature fronts and chlorophyll a in the western South Atlantic. *J. Geophys. Res.: Oceans* 110 (C11).
- Schlosser, V., Aquino, F.E., Reis, P.A., Simões, J.C., 2020. Antarctic Atmospheric Circulation Anomalies and Explosive Cyclogenesis in the Spring of 2016. *Theoretical and applied climatology*.
- Schumann, E.H., 1983. Long-period coastal trapped waves off the southeast coast of Southern Africa. *Continent. Shelf Res.* 2 (2–3), 97–107.
- Shechetkin, A.F., McWilliams, J.C., 2005. The Regional Ocean Modeling System: a split explicit, free-surface, topography-following coordinates ocean model. *Ocean Model.* 9, 347–404.
- Shechetkin, A.F., McWilliams, J.C., 2009. Correction and Commentary for “Ocean Forecasting in Terrain-Following Coordinates: formulation and Skill Assessment of the Regional Ocean Modeling System” by Haidvogel et al., *Journal of Computational Physics*. 227, 3595–3624. *J. Comput. Phys.* 228, 8985–9000.
- Skamarock, W.C., Klemp, J.B., Dudhia, J., Gill, D.O., Barker, D.M., Duda, M.G., Huang, X. Y., Wang, W., Powers, J.G., 2008. A description of the Advanced Research WRF version 3. NCAR Tech. Note NCAR/TN-475+STR 113.
- Souza, R.B., Robinson, I.S., 2004. Lagrangian and satellite observations of the Brazilian Coastal Current. *Continent. Shelf Res.* 24, 241–262.
- Stech, J.L., Lorenzetti, J.A., 1992. The response of the South Brazil bight to the passage of wintertime cold fronts. *J. Geophys. Res.* 97 (C6), 9507–9520. <https://doi.org/10.1029/92JC00486>.
- Strub, P.T., James, C., Combes, V., Matano, R.P., Piola, A.R., Palma, E.D., Saraceno, M., Guerrero, R.A., Fenco, H., Ruiz-Etcheverry, L.A., 2015. Altimeter-derived seasonal

- circulation on the southwest Atlantic shelf: 27, 8-43, 8°S. *Journal of Geophysical Research - Oceans* 120.
- Sun, X., Cook, K.H., Vizy, E.K., 2017. The South Atlantic subtropical high: climatology and interannual variability. *J. Clim.* 30 (9), 3279–3296.
- Taguchi, B., Nakamura, H., Nonaka, M., Komori, N., Kuwano-Yoshida, A., Takaya, K., Goto, A., 2012. Seasonal evolutions of atmospheric response to decadal SST anomalies in the North Pacific subarctic frontal zone: observations and a coupled model simulation. *J. Clim.* 25 (1), 111–139.
- Tang, Y.M., Grimshaw, R., 1995. A modal analysis of coastally trapped waves generated by tropical cyclones. *J. Phys. Oceanogr.* 25 (7), 1577–1598.
- Thompson, K.R., 1981. The response of Southern North Sea elevation to oceanographical and meteorological forcing. *Estuar. Coast Shelf Sci.* 13, 287–301.
- Thompson, R., 1983. Low-pass filters to suppress inertial and tidal frequencies. *J. Phys. Oceanogr.* 13 (6), 1077–1083.
- Tilburg, C.E., Garvine, R.W., 2004. A simple model for coastal sea level prediction. *Weather Forecast.* 19 (3), 511–519.
- Truccolo, E.C., Franco, D., Schettini, C.A.F., 2004. The low frequency sea level oscillations in the northern coast of Santa Catarina, Brazil. *J. Coast Res.* 547–552.
- UHSLC, 2022. Legacy data portal. <https://uhslc.soest.hawaii.edu/>.
- Veleda, D., Araujo, M., Zantopp, R., Montagne, R., 2012. Intraseasonal variability of the North Brazil Undercurrent forced by remote winds. *J. Coast Res.* 117, C11024 <https://doi.org/10.1029/2012JC008392>.
- Vennell, R., 2010. Resonance and trapping of topographic transient ocean waves generated by a moving atmospheric disturbance. *J. Fluid Mech.* 650, 427–442.
- Vilibić, I., 2008. Numerical simulations of the Proudman resonance. *Continent. Shelf Res.* 28 (4–5), 574–581.
- Wallace, J.M., Hobbs, P.V., 1977. *Atmospheric Science: an Introductory Survey*, vol. 467. Academic Press, Inc, London.
- Warner, J.C., Sherwood, C.R., Signell, R.P., Harris, C., Arango, H.G., 2008. Development of a three-dimensional, regional, coupled wave, current, and sediment-transport model. *Comput. Geosci.* 34, 1284–1306.
- Wienders, N., Arhan, M., Mercier, H., 2000. Circulation at the western boundary of the South and equatorial atlantic: exchanges with the ocean interior. *J. Mar. Res.* 58, 1007–1039.
- Williams, D.A., Horsburgh, K.J., Schultz, D.M., Hughes, C.W., 2021. Proudman resonance with tides, bathymetry and variable atmospheric forcings. *Nat. Hazards* 106, 1169–1194.
- Woollings, T., Gregory, J.M., Pinto, J.G., Reyers, M., Brayshaw, D.J., 2012. Response of the North Atlantic storm track to climate change shaped by ocean–atmosphere coupling. *Nat. Geosci.* 5 (5), 313–317.
- Wunsch, C., Stammer, D., 1997. Atmospheric loading and the oceanic “inverted barometer” effect. *Rev. Geophys.* 35 (1), 79–107.
- Yao, T., Freeland, H.J., Mysak, L.A., 1984. A comparison of low-frequency current observations off British Columbia with coastal-trapped wave theory. *J. Phys. Oceanogr.* 14 (1), 22–34.
- Zambon, J.B., He, R., Warner, J.C., 2014. Investigation of hurricane Ivan using the coupled ocean–atmosphere–wave–sediment transport (COAWST) model. *Ocean Dynam.* 64 (11), 1535–1554.
- Zenbruski, S., Barreto, T.H., Palma, J.C., Milliman, J.D., 1972. Preliminary study of geomorphological provinces of the Brazilian continental margin. *Brazilian Congress of Geology* 2, 187–209.